THERMAL ANALYSIS OF GRAY CAST IRON BY INTERPRETATION OF COOLING CURVES

A THESIS SUBMITTED TO
THE GRADUATE SCHOOL OF NATURAL AND APPLIED SCIENCES
OF
MIDDLE EAST TECHNICAL UNIVERSITY

BY

ARDA ÇETİN

IN PARTIAL FULFILLMENT OF THE REQUIREMENTS FOR THE DEGREE OF
MASTER OF SCIENCE
IN
THE DEPARTMENT OF METALLURGICAL AND MATERIALS ENGINEERING

SEPTEMBER 2002

Approval of the Graduate School of Natural and Applied Sciences

Prof. Dr. Tayfur Öztürk
Director

I certify that this thesis satisfies all the requirements as a thesis for the degree of Master of Science.

Prof. Dr. Naci Sevinç
Head of the Department

This is to certify that we have read this thesis and that in our opinion it is fully adequate, in scope and quality, as a thesis for the degree of Master of Science.

Assoc. Prof. Dr. Ali Kalkanlı
Supervisor

Examining Comitee Members

Assoc. Prof. Dr. Ali Kalkanlı

Prof. Dr. Ekrem Selçuk

Prof. Dr. İshak Karakaya

Prof. Dr. Filiz Sarıoğlu

Assoc. Prof. Dr. Tamer Özdemir

ABSTRACT

THERMAL ANALYSIS OF GRAY CAST IRON
BY INTERPRETATION OF COOLING CURVES

Çetin, Arda
M.Sc., Metallurgical and Materials Engineering
Supervisor: Assoc. Prof. Dr. Ali Kalkanlı

September 2002, 91 Pages

The aim of the present work is to investigate the relations between data obtained from the cooling curve and its first and second derivatives and the as-cast microstructure of gray cast iron, assuming that the cooling curve reflects the complete history of the solidification process. Fourteen different alloy compositions are prepared in order to obtain statistical predictive models to relate cooling curve parameters with the solidification variables such as chemical analysis, inoculation, graphite shape, primary and eutectic structures, all of which will be discussed by means of potential applications of regression equations.

A program is written in Mathcad in order to process the thermal data for plotting the cooling curve, its first and second derivatives for calculation of critical temperatures on the cooling curve. Further analysis of the data consisted of calculation of the rate of heat of solidification at every time

step for both primary dendrites and the eutectic and calculation of heats of primary and eutectic solidification by means of numerical integrations.

Keywords: Gray Cast Iron, Cooling Curve, Primary Solidification, Eutectic Solidification, Heat of Solidification.

ÖZ

GRİ DÖKME DEMİRİN SOĞUMA EĞRİLERİNİ YORUMLAMA YOLUYLA TERMAL ANALİZİ

Çetin, Arda
Yüksek Lisans, Metalurji ve Malzeme Mühendisliği
Tez Yöneticisi: Doç. Dr. Ali Kalkanlı

Eylül 2002, 91 Sayfa

Bu çalışmanın amacı, soğuma eğrilerinin katılaşmaya dair bütün bilgileri yansıttığını farzederek, soğuma eğrisi ve birinci ve ikinci türevlerinden elde edilen verilerle gri dökme demirin mikroyapısı arasındaki bağlantıları araştırmaktır. Soğuma eğrisindeki değişkenlerle kimyasal analiz, aşılama, grafit tipi, birincil ve ötektik yapılar gibi katılaşmaya bağlı değişkenler arasındaki istatistiksel bağlantıların regresyon denklemleriyle bulunması amacıyla ondört farklı alaşım kompozisyonu kullanılmıştır.

Dökümlerden elde edilen sıcaklık verilerinden soğuma eğrilerini ve birinci ve ikinci türevlerini hesaplayarak kritik sıcaklıkları bulmak için Mathcad kullanılmıştır. Verilerin daha detaylı analizi, birincil ve ötektik katılaşma süresindeki her zaman diliminde katılaşma hızının hesaplanması ve

nümerik integrasyonla birincil ve ötektik katılaşmalardan yayılan ısıların hesaplanmasını içermektedir.

Anahtar Kelimeler: Gri Dökme Demir, Soğuma Eğrisi, Birincil Katılaşma, Ötektik Katılaşma, Katılaşma Isısı.

To My Family

ACKNOWLEDGMENTS

I would like to offer my apprecation to Assoc. Prof. Dr. Ali Kalkanlı for his guidance and insight throughout the research. I also express sincere apprecation to Prof. Dr. Ekrem Selçuk and Prof. Dr. Nevin Selçuk for their directions and suggestions.

I want to thank in advance to Haluk Güldür from Heraus Electo-Nite, Erdoğan Nas, İlknur Uysal and Hamdi Paşaoğlu from Erkunt A.Ş. and Ümit Çağlayan from Extra Metal for their consideration, supplements and contribution to this work.

The technical assistance of Salih Türe and Yaşar Kazanç is gratefully acknowledged.

To Ozan Bilge, Fatih Güner, Süha Tirkeş, Ersin Emre Ören and Fırat Tiryaki, I express sincere thanks for their support and assistance in every part of this research.

Finally, thanks go to Ziggy Zinc for providing continious motivation and endurance in every aspect of the present thesis.

TABLE OF CONTENTS

LIST OF TABLES

TABLE

LIST OF FIGURES

FIGURE

CHAPTER 1

INTRODUCTION

It is accepted that under the same thermodynamic conditions, specimens of the same material can be expected to behave in the same way at the same temperature. Thus, the ability to record and analyze the whole solidification process using cooling curves should allow the prediction of the final structure of the specimen. Thermal analysis is a very valuable tool for evaluation of the solidification characteristics of cast iron melts that has found application in both fundamental research investigations and in foundry, for control of molten metal processing. Over the past decade, rapid progress has been made in the development of various mathematical models simulating the solidification of cast irons. Most of the effort has focused on the calculation of the amount and the rate of latent heat of eutectic solidification with the aid of simple temperature dependent solidification models. Primary solidification has remained rather undiscussed and all parameters regarding the mechanical properties of cast iron has related to eutectic solidification.

It is well recognized that the type and morpholgy of phases formed during the solidification of cast irons is a function of both nucleation and growth stages. Yet, these aspects of the solidification process are less well understood for cast irons for most other commercial alloys, in part due to the compexities encountered in these alloy systems.

Although it is recognized that the solidification of cast irons is clearly influenced by the various constitutients that are normally present in the melt, and that undercooling plays a significant role in determining the solidification structures that develop, little is known or understood regarding the basic physical mechanisms and details of the kinetics that govern the influence of undercooling on solidification.

As mentioned in the lately published papers and confirmed by the results of the present research the mechanical properties of gray cast iron is principally determined by the primary solidification. Eutectic solidification also plays a significant role. The role of thermal analysis is to investigate the relationships between those solidification parameters and thermal data by interpretation of cooling curves.

This work presents the cooling curves and their first and second derivatives for fourteen different cast iron compositions, heats of primary and eutectic solidifications, the metallographic examination and tensile strength results and investigate the relation of those parameters with cooling curves by potential applicaltion of multiple regression equations.

CHAPTER 2

THEORY

2.1 Metallurgy of Cast Iron

Cast iron is a very fickle material that finds wide acceptance in the industry. It represents about 70% of the total production of the castings world wide. It is possible to produce castings with high strength and hardness, although brittle, or with low strength and hardness and high ductility. In the case of ADI (Austemper Ductile Iron), it is possible to obtain very high strength and ductility. In most circumstances, this could be achieved by starting from the same molten metal to which small amounts of some elements are added, or by a variaton of the cooling rate during solidification or solid state transformation. On the other hand, it is possible to attain in the same casting, with complex shape and sections with quite different thickness, parts that solidify in accordiance with the stable diagram and other parts according to the metastable reaction.[1]

2.1.1 The Iron – Carbon Phase Diagram

Although castings rarely solidify under equilibrium conditions, phase diagrams can be of considerable value for predicting the microstructural changes that occur during and after solidification.[2] The constitution phase diagram of the iron - carbon system (Fig. 1) has been constucted by

collecting and plotting thermal data. This diagram deals only with the constitution of the system; i.e., what phases are present and how much of each is present, and not with their structure. In the diagram, temperature is plotted vertically and composition horizontally. Any point on the diagram, therefore represents a definite composition and temperature, each value being found by projecting to the proper reference axis.[3] The two diagrams in Fig. 1 are for the stable iron - graphite and metastable iron – iron cemetite systems. The phase diagram provides a unique capability for analysis and understanding of the effects of alloying elements on solidification processes of Fe-C based alloy systems.

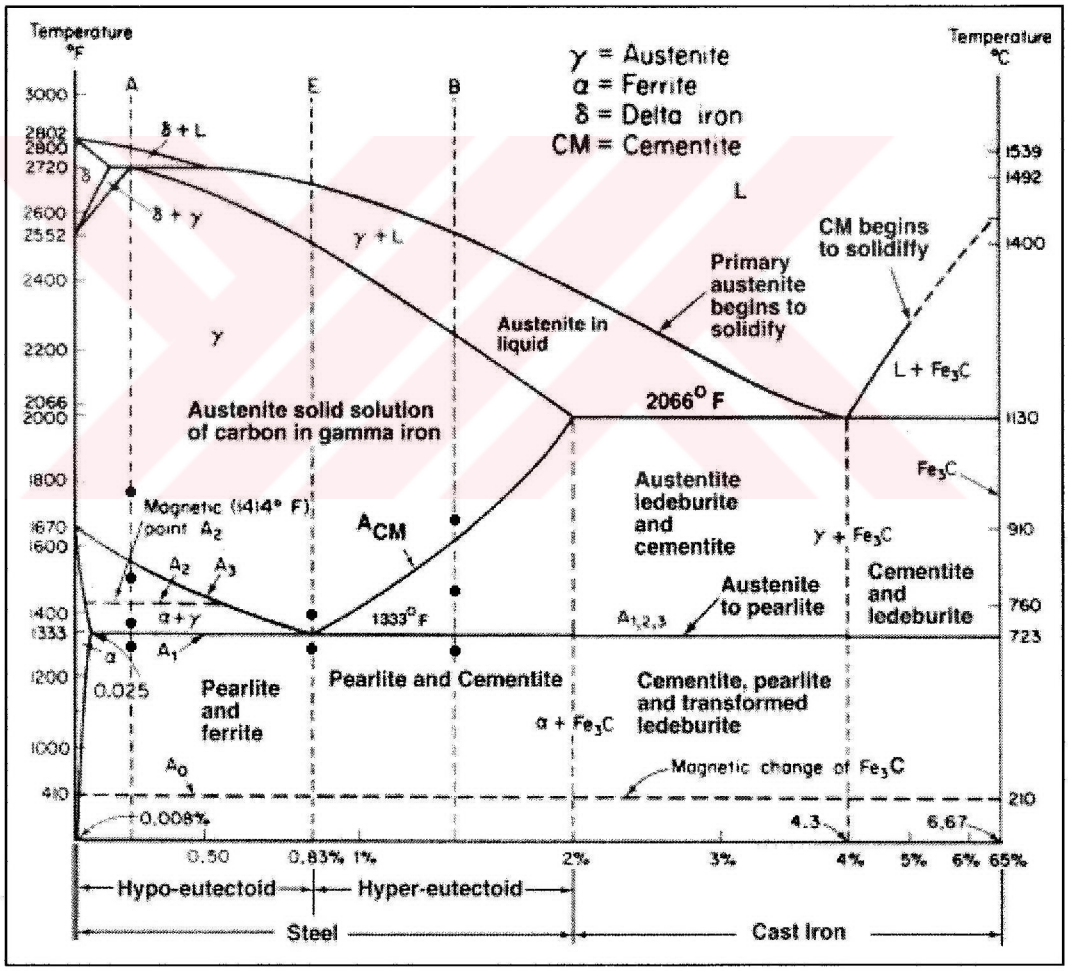

Fig. 1. The iron – carbon phase diagram

2.1.2 Classification of Cast Irons

White Cast Irons, in which all of the carbon is present as cemetite, and the structure may be interpreted in terms of the metastable system iron - cementite.

Gray Cast Irons, in which a substantial part of the carbon is present as graphite, and some transformations involve the stable system iron - graphite.

Mottled Cast Irons, are intermediate between white and gray cast irons and contain some graphite and some eutectic cementite.

Malleable Cast Irons, are alloys which are cast as white irons, and then heat - treated, either to decompose the iron carbide to give graphitic nodules, or under conditions where the carbon is removed by oxidation.[4]

2.1.3 Gray Cast Iron

Gray iron itsself a family of casting alloys, and is the most popular, with annual production several times the total of all other cast materials. The name was derived from the characteristic gray color of the metal which is due to the contained flakes of graphite.[5]

The gray cast irons contain much of the carbon in the form of graphite, and thus involve the stable, as well as the metastable equilibrium diagram. Most gray cast irons contain so much silicon that their structures are often reffered to the equilibrium diagram of the ternary system Fe-Si-C.[4]

The solidification of a hypoeutectic gray cast iron under conditions resembling those of the stable equilibrium diagram involves first the

formation of primary dendrites of austenite, followed by the binary complex. The solidification of the latter takes place in a cellular form in which the graphite is present in the form of thin flakes whose surfaces are roughly parallel to the close - packed planes of carbon atoms. These eutectic cells may be regarded as growing outwards untill they fill the interdendritic space.[4]

In the hypereutectic cast irons, it is well known that when the carbon content is high, graphite known as *kish* readily seperates, and floats to the top of the melt is the temperature is not kept sufficiently high. This graphite is in the form of flakes whose flat surfaces are parallel to the hexagonal layers of the crystal structure. In a hypereutectic gray cast iron, the primary of proeutectic graphite is in the form of thin plates.[4]

2.1.4 The Iron – Carbon – Silicon System

The basic composition of cast iron alloys having flake graphite as a structural element is Fe - C - Si. Typical vertical sections of the Fe - C - Si system are shown in Fig. 2. These sections show that the C content of the eutectic decreases with increasing Si content, while eutectic temperature steadily decreases.

A convenient way of representing the influence of Si on the different structures in the Fe - C - Si system is by a Maurer diagram, as shown in Fig 3.

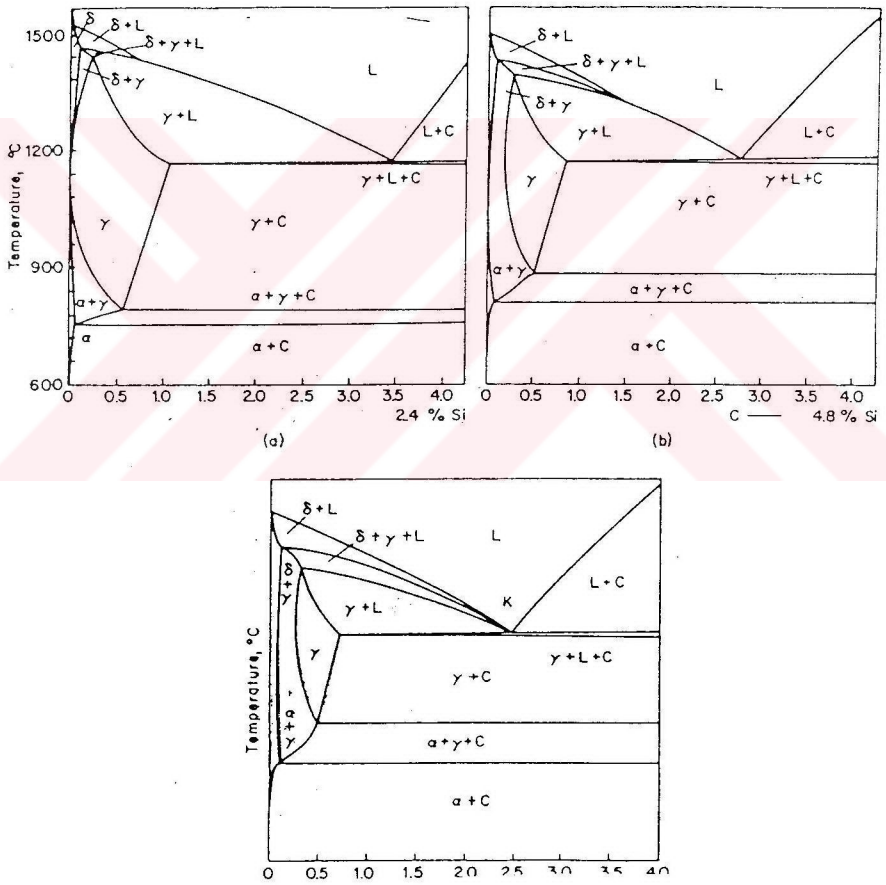

Fig. 2. Vertical sections in Fe-C-Si system

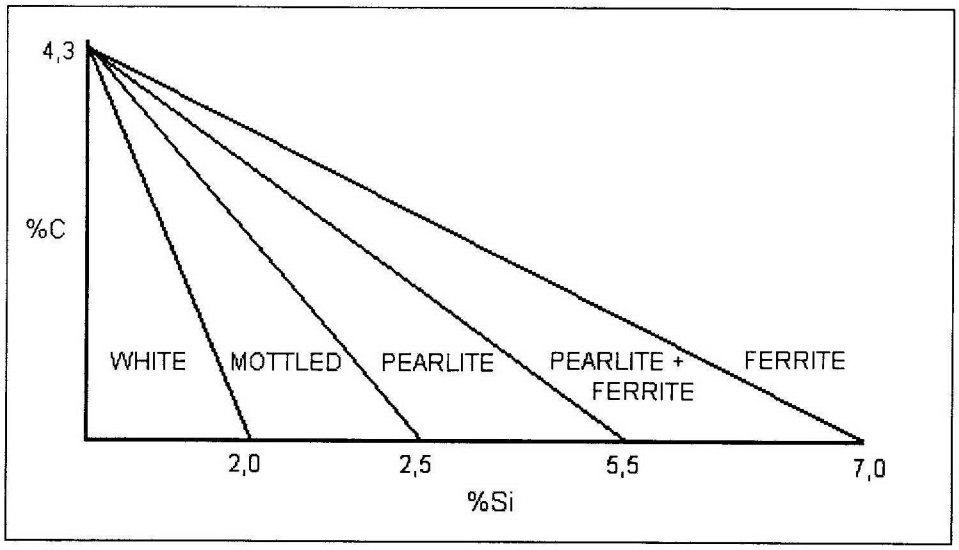

Fig. 3. Maurer diagram

Ordinary Fe -C cast alloys would solidify according to the metastable system and the structure would be white. As Si is increased in content, the structure changes from a white mode, through mottled to a flake structure. In the process, the matrix structure also changes from a pearlitic one, to pearlite and ferrite, and finally to ferrite.[6]

2.1.5 Effect of Silicon on Transition from Metastable to Stable System

The transition of the solidification of Fe-C-Si alloys from the stable to the metastable system can be explained in terms of differences in nucleation temperatures of the graphite and cementite phases as well as in the growth rates of the two eutectics. Fig. 4 shows a schematic temperature – growth rate diagram for the stable Fe-C and the metastable Fe-Fe_3C systems. The diagram illustrates two main points:

(i) the graphite can be nucleated at higher temperatures than the cementite

(ii) below a critical temperature, the growth rate of graphite becomes much slower than that of Fe_3C.

From this diagram, it becomes clear that, provided no difficulties in nucleation exist, graphite will always be formed at the beginning of the solidification. If the cooling rate is low, the solidification will be completed before the nucleation temperature of Fe_3C is reached, and a completely gray casting will result. At high cooling rates, the bath temperature will drop below T_{crit}, and the Fe-Fe_3C eutectic will overgrow the graphite eutectic. The result is then a mottled or a white structure. Nucleation difficulties for either the graphite or the cementite will induce kinetic effects which may be influenced by techniques such as overheating of the melt or inoculation.

The main effect of silicon is an increase in the gap between the stable and the metastable eutectic equilibrium temperatures. Fig. 4 shows how the temperature – growth rate diagram is influenced by silicon. The slope of the growth rate curves is slightly changed by silicon.[7]

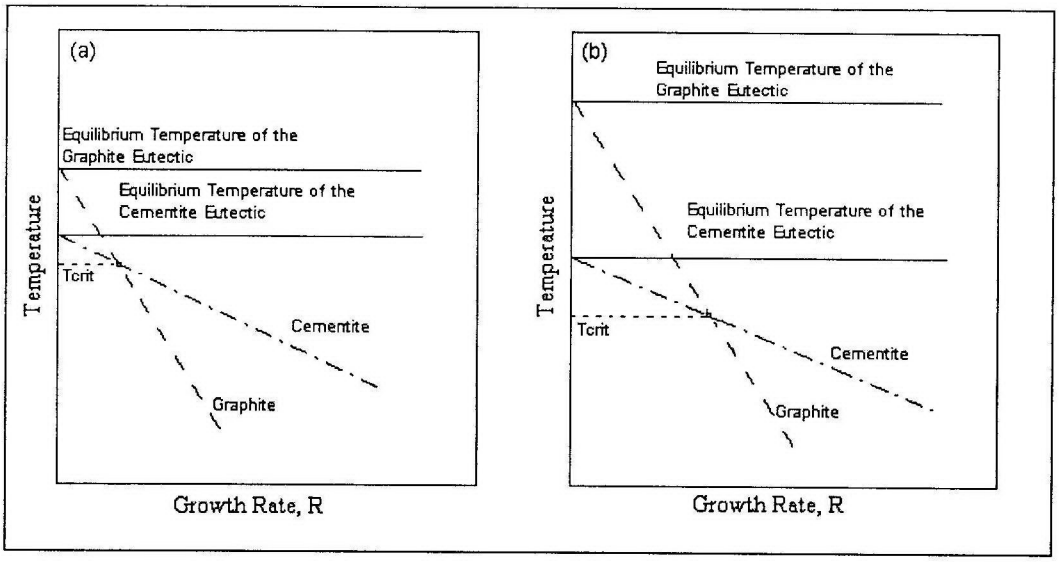

Fig. 4. Schematic representation of the growth rate of the graphite and cementite eutectics of Fe-C-Si alloys as a function of the temperature, (a) with low Si content, (b) with increased Si content

2.1.6 Carbon Equivalence

Carbon equivalence (CE) is a very valuable number for evaluating the effect of composition in cast irons. Carbon equivalence is determined by simply adding one - third of the sum of silicon and phosphorus contents to carbon content of the cast iron:

$$CE = \%C + (\%\ Si + \%\ P) / 3$$

The evaluation of the cast iron can be done by comparison of CE with the eutectic composition in the Fe - C system (4.3% C). If CE is greater than about 4.3% C, the cast iron is said to be hypereutectic, and if CE is lower than about 4.3% C, then the cast iron is said to be hypoeutectic.

Another significant relationship that defines the composition of cast iron in terms of carbon, silicon and phosphorus is the carbon equivalent liquidus (CEL) given by,

$$CEL = \% C + \% Si / 4 + \% P / 2$$

2.2 Inoculation of Gray Cast Iron

Inoculation is a means of controlling the structure and properties of cast iron by minimizing undercooling and increasing the number of nucleation events during solidification.[8]

The inoculation of cast iron involves the addition of small amounts of certain materials (inoculants) to the molten metal, either just before or during pouring.[9] The effect is usually time - dependent since the added substances tend to dissolve in the melt.[10] Common inoculants are graphite, and high silicon materials such as ferrosilicon and calcium silicide. A number of proprietary inoculants based on one or more of these materials are also available. It is necessary to inoculate many gray iron castings and almost all nodular (SG) iron castings, to avoid the formation of eutectic carbide or 'chill' in thin sections and to improve mechanical properties. Inoculation provides new or additional nuclei from which growth of the eutectic can take place, and this effect is often described as increasing the degree of nuclation of an iron.[9] Inoculation thus influences the number and size of cells and also the carbon precipitation. The number of cells has an effect not only in physical properties but also on the castability of the alloy. Too high a cell count in gray iron might e.g. increase the tendency for microshrinkage, especially in green sand molds. With a sufficient number of nuclei the solidification can start at a low undercooling. The dissolved carbon can thereby precipitate as graphite instead of forming cementite, as the distances for diffusion are short. The

amount of graphite will be high, which means that the associated expansion might offset the contraction of the austenite if properly balanced.[11]

2.2.1 The Purpose of Inoculation

The purpose of inoculation is to aid in providing enough nucleation sites for the carbon to precipitate as graphite rather than iron carbide (cementite, Fe_3C). This means to prevent undercooling to temperatures below the metastable eutectic where carbidic structures are formed.[12]

The principal effects of inoculation of gray cast iron are as follows:

(a) Reduces chill and promotes graphite formation.
(b) Reduces the formation of fine graphite such as Type D and associated ferrite.
(c) Promotes uniform structures in various sections.
(d) Tends to increase strength.
(e) Enables high-strength irons of low carbon equivalent to be cast free from chill.
(f) Increases tendency to unsoundness.[9]

2.2.2 Monitoring of Inoculation of Gray Cast Irons

Cooling curves for gray irons typically demonstrate undercooling below the graphite eutectic temperature and a subsequent recalescence when the eutectic nucleates and propagates at a rapid rate, releasing its heat of fusion. The recalescence measured for a gray iron would seem to reflect the driving force possessed by that iron for the nucleation and growth of the stable graphite eutectic. For this reason, it has been suggested that recalescence measurements taken from the cooling curves of samples poured into standard eutectometer cups without tellerium could be used to monitor and control the inoculation of gray irons.

For example, if a sample of furnace iron demonstrates a large recalescence, then its graphitizing tendency might be strong and less inoculant might be required in the pouring ladle or in-stream at the mold. Conversely, a low recalescence might require a heavier inoculation of the iron. A technique such as this would allow more control to be exercised over the casting process.[13]

Another important parameter for monitoring the inoculation of gray cast iron from cooling curve, which is illustrated in Fig. 5 is the minimum eutectic temperature ratio (UQ) between the inoculated and uninoculated samples. The ratio of the minimum eutectic temperature of uninoculated sample (Tu) to the minimum eutectic temperature of inoculated sample (Ti) is defined as;

$$UQ = Tu / Ti$$

An UQ value between 1,5 and 2,5 indicates good inoculation. If UQ is lower than 1,5 there is insufficient inoculation whereas an UQ value greater than 2,5 points out excessive inoculation, which is a waste of inoculant material.

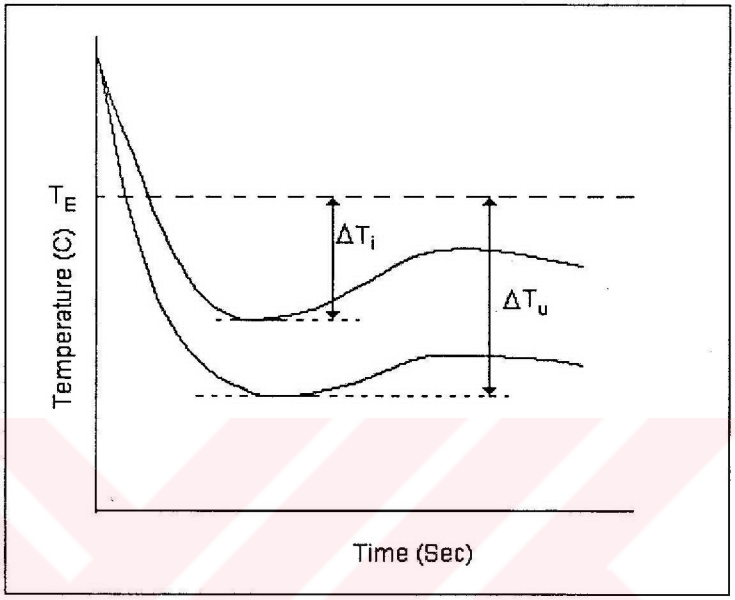

Figure 5. Monitoring of inoculation from cooling curve

2.2.3 Effects of Inoculation on Cooling Curve

The first temperature that is influenced by inoculation is the liquidus temperature. The inoculant acts as a deoxidizer. If the iron contains a high amount of oxygen, the carbon activity is reduced and an increase in the liquidus temperature can be recorded. If such an iron is inoculated, the liquidus temperature is sometimes reduced with 8 – 10 °C.

Also the plateau at liquidus temperature which partly represents exogeneous growth of dendrites is influenced by nucleation. The most pronounced effect however, is on the minimum eutectic temperature and

the maximum eutectic temperature. Normally, the minimum eutectic temperature is raised more than the maximum eutectic temperature so that also the recalescence is reduced.

Other parts of the curve that show a distinct response to inoculation are start of eutectic freezing, maximum recalescence rate, and first derivative at solidus.[11]

2.2.4 Inoculating Materials

Typical compositions of some inoculants are given in Table 1.

Table 1. Typical compositions of some inoculants.[9]

Type of Inoculant	Si%	Al%	Ca%	Ba%	Sr%	Zr%	Mn%	Mg%	Ti%	C%
FeSi	75-80	1.2-2	0.3-1.2							
FeSi-Mn-Zr (SMZ)	60-65	1-2	1-3			5-6	5-6			
FeSi-Ba FeSi-Ba FeSi-Ba	60-65 60-65 60-65	1.0 0.5-1.7 1.5	08 1.0 2.0	0.8 9-11 5-6		6	6 9-10			
FeSi-Zr	80	1.5-2.5	2.5			1.5				
FeSi-Sr FeSi-Sr	75 45-50	<0.5 <0.5	<0.1 <0.1		0.8					
FeSi-Ti	45-50	1.5	6		0.8				10	
FeSi-Ce	45	0.5	0.5							
Ca-Si	60	1-2	30							
Low cost 45% FeSi	45-50	0.8	0.8							

Table 1. Typical compositions of some inoculants[9] (Continued)

Type of Inoculant	Si%	Al%	Ca%	Ba%	Sr%	Zr%	Mn%	Mg%	Ti%	C%
FeSi-La	75	1.5								
Graphite										98 - 99.9
FeSi + Graphite	40-50	1.0	1.5							45

2.3 Gray Solidification of Cast Iron

The gray or white solidification mode of cast iron is dependent on the relative nucleation possibility and growth rates of the graphite and cementite phases. This will depend on alloy chemistry of the melt and on the phase growth in the conditions established.[14]

From practical experience it is well known that a cast iron melt mey be made solidify gray by slow cooling and white by rapid cooling. This observation has led to the conclusion that each cast iron has a certain critical cooling rate below which it solidifies completely gray and a higher critical cooling rate above which it solidifies completely white. Between the two critical rates a mottled structure is formed.[15]

The graphite and the carbide phase equilibrium phase equilibrium region leads to two eutectics. The stable eutectic between austenite and graphite phases lies slightly above the metastable eutectic between austenite and cementite. This temperature difference depends on the alloy content. Between these temperatures only the graphite eutectic can nucleate and grow.

2.3.1 Stable and Metastable Systems

For two components, Fe-C, only three phases are permittes at a constant temperature of binary eutectic solidification. These are Fe + Gr + melt in the stable system and Fe + Fe_3C + melt in the metastable system. The occurence of double eutectic arrests and/or eutectic freezing over a temperature range also violates the requirement of constant eutectic temperature freezing in a binary system. These violations are resolved by conventional arguments to the effect that stable and metastable systems are superimposed and that impurities are present so that the alloys are not truly binary. Further, it is usually stated that the kinetics of nucleation and growth are acting to prevent the phase equilibrium reactions from occuring at the expected temperatures and/or compositions. Transformation diagrams may be used to present phase reactions in a way which includes some of the kinetic factors.[16]

2.3.2 Solidification Sequence

Many processing variables influence the microstructure and properties, including type of melting furnace, charge materials, melt history (temperature, time and superheat), degree of oxidation, pouring temperature, type of inoculant, form and method of inoculant addition, and solidification rate of the metal. The variety of factors that influence iron solidification makes it important for foundrymen to exert good process control.[17]

In the solidification process, as the temperature of the liquid metal falls below the melting point, nucleation begins. Crystal clusters (or embryos) are formed. These clusters may melt or grow. When the clusters are big enough, they will not melt any more. At this time, they are called nuclei. At the beginnig of nucleation, the number of nuclei increases very slowly.

After a critical undercooling value is reached, the number increases rapidly. Nucleation proceeds until the decreasing temperature starts to increase, i.e., recalescence occurs. At this point, the number of nuclei reaches its maximum value.

After nucleation, there is a long period of growth. In this step, the grain radii increases continuously until the grains come into contact with one another, and this is followed by the third step; impingement. In the final step, through the grain radii can not increase any more, there is still some liquid metal among or inside the grains, which will solidify in this step.[18]

It is well recognized that the mastery of the type and morphology of phases formed during the solidification of cast irons is a function of both nucleation and growth stages of solidification. Yet, these aspects of solidification process are less well understood for cast irons than for most other commercial allys, in part due to the complexities encountered in these alloy systems. Not only are cast iron alloys multicomponenet systems, but solidification and transformation of these alloys is well established to occur in both the stable (graphite) and metastable (carbide) systems. Accordingly, it has been difficult to conduct studies that characterize the nucleation and growth kinetics involved in either Fe-C-Si alloys or in commercial cast irons.[19]

2.3.3 Heterogeneous Nucleation

Most interpretations of heterogeneous nucleation are based on the concept that the lattice misfit between the nucleant and the nucleating solid determines the amount of undercooling required for the onset of nucleation. With increasing misfit, increasing undercooling is realized. Using data for the lattice parameters of the phases in the temperature range of interest, the registry of the interface between the (0001) of

graphite and the (111) of austenite is depicted in Fig. 6. The planar disregistry between the planes (about 4.55%) is small enough so that one could expect only a small undercooling for nucleation of austenite by graphite.

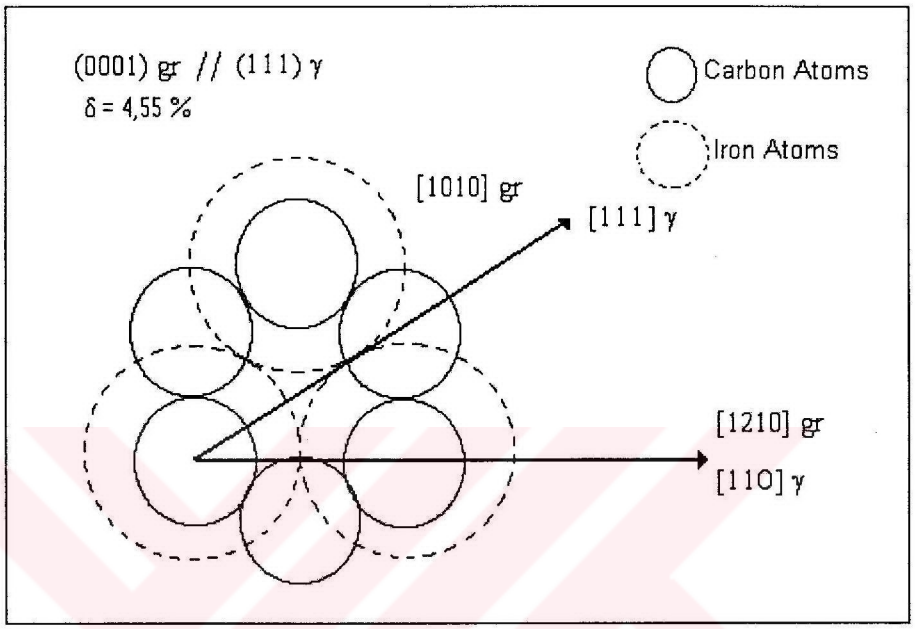

Figure 6. Sketch illustrating the crystallographic relationship at the interface between the (0001) of graphite and the (111) of austenite. The value of δ = 4.55% represents the extent of lattice disregistry.

However, it would also be expected that the same small undercooling would be effective in austenite nucleating graphite, a condition not attained in the cooling of hypoeutectic alloys. Furthermore, it is recognized that the complex orthorhombic structure of Fe_3C contains a (100) plane that is semicoherent with the (111) plane of austenite. It would follow then that, on the basis of the theory of lattice misfit, austenite should readily nucleate Fe_3C, and that Fe_3C should readily nucleate austenite. But considerable undercooling was required before the carbidic eutectic was nucleated.[19]

Favorable intefacial energy generally signifies that the energy between the nucleant surface and the melt should be larger than that between the nucleating product phase and the melt. In this case, the formation of the product nucleus is promoted on the catalyst-melt interface. Moreover, the difference between these solid-liquid interface energies should be greater than the solid-state interface energy between the product phase and the nucleant. This condition is favored for a low disregistry, which promotes good crystallographic matching and coherent interfaces. To assure good coherency:

$$\cos \theta = (\sigma_{LN} - \sigma_{SN}) / \sigma_{LS} \geq -1 \qquad (1)$$

where θ is the contact angle, σ_{LN} is the liquid/nucleant interfacial energy, σ_{SN} is the nucleating solid/nucleant interfacial energy, and σ_{LS} is the liquid/nucleating solid interfacial energy. If $\sigma_{SN} \geq 2\sigma_{LN}$ (which is typical for solid/solid interfaces such as large grain boundary energies), the value of $\cos \theta$ will be less than –1. Heterogeneous nucleation would never occur on the planes of a nucleant that possessed large solid/solid interfacial energies, but is favored for a low disregistry that promotes good crystallographic mathching and coherent interfaces.

Another approach, requires that the liquid/nucleant interfacial energy, σ_{LN}, be greater than the liquid/nucleating solid interfacial energy, σ_{LS}. If the surface of the nucleant is coated with a thin coherent, or semicoherent, layer of solid at the liquid/ nucleant interface, the energy of the system will be lowered. Thus, the interfacial energy between graphite and cast iron melt should be greater than that between austenite and the cast iron melt.

It can, therefore, be concluded that, in cast irons, inoculants having a larger interfacial energy than graphite, with respect to the liquid, and that are coherent or semicoherent with graphite, are favored to serve as

heterogeneous nucleants for graphite nucleation. Similarly, an effective heterogeneous nucleant for austenite must not only possess crystalline compatability but must have an interfacial energy with respect to the liquid that is larger than that of austenite. In other words, graphite will serve as an effective nucleant for austenite, but austenite is a poor nucleant for graphite.[19]

The solidification of flake graphite cast iron will start on a low number of nuclei, as compared with ductile iron, reflected in the low eutectic cell count. Since the growth conditions in the liquid are favorable, these nuclei will start growing as soon as the temperature will drop below the equilibrium temperature, with very little undercooling; i.e., both the minimum eutectic temperature and the maximum eutectic temperature will be close to the theoretical eutectic temperature and the recalescence will be very small. Within the eutectic cell the graphite will grow in contact with the liquid, mainly along the A axis of the hexagonal graphite crystal, resulting in graphite plates, more or less branched.[20]

2.3.4 Factors Affecting Nucleation

Nucleation properties are influenced by numerous factors, such as;

1. The charge composition
2. Amount of combined carbon in the charge
3. Size of the charge materials
4. Rust level
5. Charging sequence
6. Time and temperatures during melting and holding
7. Number of overpours before reaching the pouring ladle.[11]

Moreover, it should be mentioned that sulphur changes the contact angle between liquid cast iron and graphite which influences critical radius. In addition, when the solid is allowed to be transported by the convection currents, the total number of grains increases. This effect is due to the fact that the highly supercooled liquid – solid mixture is transported from the peripheral layer towards the thermal center of casting. In a similar way relatively warm metal, coming from the center of the casting where nucleation is less favorable, because of the lower supercooling, is cooled down at the mould wall which increases the number of available nuclei. The equiaxed solidification mode of both cast iron types allow this mechanism; however it is not known at which solid fraction the convection currents will be hindered.[21] All these effects make it very difficult to construct a mathematical model for nucleation step.

2.3.5 Solidification of Hypoeutectic and Hypereutectic Gray Cast Irons

Solidification of hypoeutectic gray cast iron starts with the formation of austenite dendrites when the temperature falls below the equilibrium liquidus. Because C diffuses very rapidly in Fe, and because nucleation of austenite is not difficult, the fraction of primary austenite solidified is related to the temperature through the inverse lever rule. This may be written as

$$f_s = (1 / 1 - k').(T - T_L / T - T_\gamma) \qquad (2)$$

where k' is the ratio of the slope of the liquidus curve to the slope of the solidus curve, T_γ is the temperature at which the interpolations of those curves intersect, and T_L is the liquidus temperature. It is more convenient in the work which follows to use the expressions for solidification rate.

Differentiating Eqn. (2) yields

$$df_s/dt = (1 / 1 - k').(T_L - T_\gamma / T - T_\gamma)^2.dT/dt \qquad (3)$$

for $T_L \geq T \geq T_E$

Nucleation of the eutectic can begin once the temperature falls below the equilibrium eutectic temperature, TE, and further nucleation and growth of existing nuclei ensues as more heat is extracted. Eventually, the latent heat released by solidification causes the temperature to rise (recalescence), after which nucleation ceases and further solidification comes solely from growth of existing particles. In most manufacturing processes, melt chemistry is controlled such that the recalescence temperature is greater than the solidification temperature of the metastable Fe – Fe_3C eutectic, preventing the formation of undesirable white cast iron. The resulting microstructure of the Fe – C eutectic consists of nominally spherical austenite cells with radial graphite flakes.[22]

Solidification of hypereutectic cast iron begins with the crystallization of primary graphite. The primary graphite develops as straight graphite plates with some branching growing while totally surrounded by liquid. The composition of remaining liquid shifths toward the eutectic, where the liquid is believed to solidify in a manner similar to that of a eutectic cell although the primary graphite may influence the size of the eutectic cell and distribution of the eutectic graphite.[23]

2.3.6 Grain Impingement

Grain impingement can occur at any time, depending on the distribution of the nuclei (random or aggregated) and the manner of growth (shape of grains and growth velocity). Grain impingement can significantly delay the growth process and affect the temperature evolution during transformation.

The effect of grain impingement has been treated by Johnson and Mehl and Avrami.[24] Assuming random nucleation sites, they derived that the real volume fraction, f, can be calculated from the extended volume fraction, f_{ex}, which is the volume fraction yielded under the condition of free growth (i.e., with no impingement). The relationship between the real volume fraction and the extended volume fraction was given as

$$df = (1 - f)\, df_{ex} \qquad (4)$$

where $(1 - f)$ is the grain impingement factor, and the extended volume fraction is equal to

$$f_{ex} = -(4.\pi / 3).N.R^3.t^4 \qquad (5)$$

The Johnson - Mehl - Avrami equaiton has four restrictions under isothermal conditions, i.e., random nucleation site, constant nucleation rate, N, constant growth rate, R, and small incubation time, τ.

Dendritic, eutectic and ferritic grains are assumed to nucleate randomly and instantaneously, and hence, the extend of impingement is not severe or even negligible at the early stage of transformation. Accordingly, the impingement factor should be included only at high volume fractions of transformed phases. The critical fraction of transformed phases where grains begin to impinge upon one another depends strongly on the shape of the grains and the type of packing. Theoretically, this value is 0.74 for spherical grains with close-packing. However, in the as-cast structure, the ferrite grains may impinge upon one another at a relatively low fraction. Therefore, an alternative factor, $(1 - f)^f$, which implies that the extend of impingement becomes more pronounced as the transformed phases increases, should be used.[24]

2.4 Undercooling in Gray Cast Irons

2.4.1 Constitutional Undercooling

If a steady-state solidification at a planar interface is considered as shown in Fig. 7. As a result of the varying solute concentration ahead of the solidification front there is a corresponding variation of the equilibrium solidification temperature, i.e., the liquidus temperature, as given by the line T_e in Fig 7. However, apart from the temperature of the interface, which is fixed by local equilibrium requirements, the actual temperature of the liquid can follow any line such as T_L. At the interface $T_L = T_e = T_3$. If the temperature gradient is less than the critical value shown in Fig. 7b the liquid in front of the solidification front exists below its equilibrium freezing temperature, i.e., it is supercooled. Since the supercooling arises from compositional, or constitional effects it is known as constitional supercooling.[25]

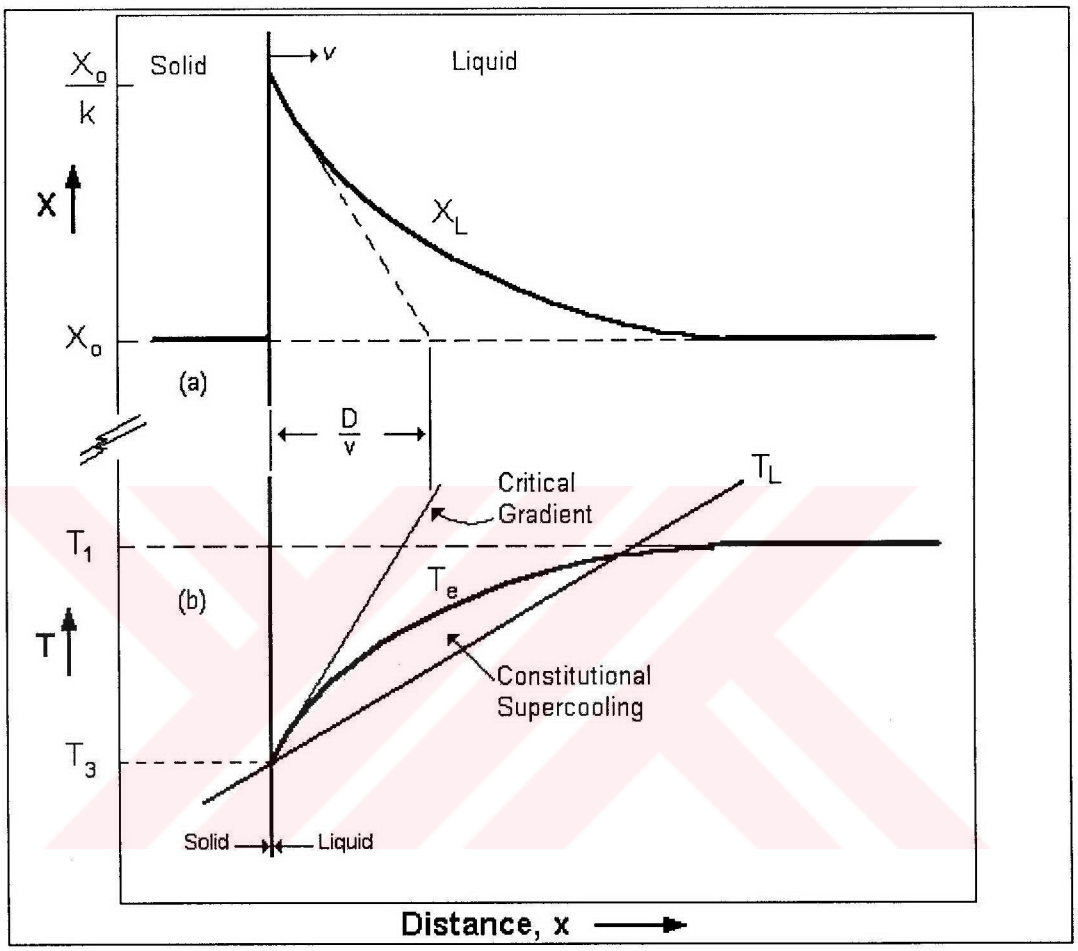

Fig. 7. The origin of constitutional supercooling ahead of a planar solidification interface.

The effects of constitutional supercooling upon the crystallization are of three types, depending upon the degree of supercooling.

1. If there is only minor supercooling, certain preferred regions of the interface will protrude as spikes into the supercooled region and, once started, will grow more rapidly than neighboring regions. This will happen both because the driving force for freezing is greater in the supercooled region and because these spikes will reject solute at their sides, thus delaying freezing of the side regions.

2. If supercooling is greater, the spikes tend to form side arms, producing a denritic structure.

3. Finally, in the case of extreme supercooling, the temperature difference may become large enough to lead independent crystallization. In this way, randomly oriented (equiaxed) grains may be encountered toward the central part of an alloy ingot.[26]

2.4.2 Other Causes of Undercooling

Many factors may interact to produce undercooling of the eutectic liquid, including high percentages of steel in the furnace charge, high dissolved hydrogen and nitrogen contents, poor nucleation, excessive holding time after inoculation, and tramp elements in the metal. Thermal analysis can be used to facilitate detection of problems, but it does not define the cause of undercooling or carbide formation.[17]

2.4.3 Undercooling in Gray Cast Irons

Several authors, amongst them Prof. Czikel and Dr. Hummer, consider the difference between the maximum and minium eutectic temperature as the eutectic undercooling. Others, like K. H. Caspers, define undercooling as the difference between a reference temperature and 1150°C and the minimum of the ideal solidus temperature of the pure binary Fe-C alloy in the stable system. Both definitions are used to correlate undercooling with the degree of nucleation of cast iron, and further to its mechanical and physical properties.[27]

2.4.4 Effect of Undercooling and Cooling Rate on Mechanical Properties

While it is recognized that the initiation of solidification of cast irons is clearly influenced by the various constituents that are normally present in the melt (including inclusions and various particulates intentionally or unintentionally added), and that undercooling plays a significant role in determining the solidification structures that develop, little is known or understood regarding the basic mechanisms and details of the kinetics that govern the influence of undercooling on solidification.[19]

The influence of very high cooling rates in producing fine structures offers the possibilty of future development of cast irons possessing high strength and fracture toughness. The undercooling of a melt to a lower temperature increases the number of effective nuclei for solidification relative to the growth rate, the latter being restricted by the rate at which the latent heat of crystallization can be dissipated. Conversely, slow cooling favors the growth from a few solidification nuclei and produces coarse grain structures. The refining effect of enhanced cooling rate applies both to the primary grain size and to the substructure, although in the latter case, the

effect is on the growth process rather than on nucleation. Thus, these is a marked effect upon dendritic grain size, cell size and microstructure over a wide range of cooling rates and, consequently on the mechanical properties.[23]

2.5 Macro and Microstructure of Gray Cast Iron

2.5.1 Dendritic Structure

Solidification over a temperature range is the primary requirement for dendrite growth. Primary austenite dendrites readily grow from the liquidus down to the eutectic temperature. Growth of dendrites may also continue, concurrently with the eutectic, as the temperature decreases through the eutectic range to the solidus. Thus, undercooling may lead to longer dendrites and higher interaction. The longer dendrites and larger percent interaction of undercooled irons explain why higher strengths were associated with lower minimum eutectic temperatures.[17]

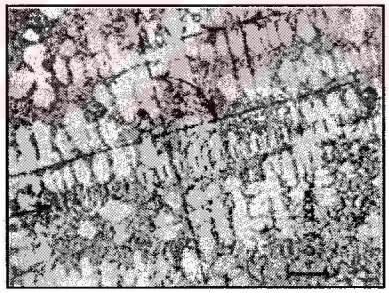

Figure 8. Dendrites observed in gray cast iron

Some recent publications have suggested that proeutectic and eutectic dendrites may be benefical in increasing strength of cast iron. This is quite logical since, most gray irons are hypoeutectic in composition and start to solidify by nucleation of primary austenite dendrites. Thus, it follows that the shape and size of the dendrites influence the type of graphite formed

and may have a more dominant effect on strength than either graphite type or eutectic cell size. The size and shape of austenite dendrites are primarily determined by the carbon equivalent, alloy content and solidification behaviour. Since dendrite growth is characterized by solidification over a temperature range, thermal analysis may be used to measure undercooling and indicate the nature of austenite dendrites.[17]

The minimum eutectic temperature can be used as a measure of cells precipitated and the chilling tendency of iron. High dendritic interaction areas in the case of chilled cast irons reflect the interweaving of dendrite through eutectic cells that effectively tie eutectic cells together.[23] Higher interaction areas reflect the interweaving of dendrites through eutectic cells that effectively tie the eutectic cells together. Since dendrites are formed from primary austenite and do not contain flake carbon, they have a higher fracture stress than eutectic liquid that decomposed to form austenite and eutectic carbon.[17]

The secondary dendrite arm spacing of the dendrites in hypoeutectic and hypereutectic irons depends on the cooling conditions and the carbon equivalent of the iron. It also appears to depend on the solidification range over which the dendrites grow (T_L – TEU), where T_L is the liquidus arrest and TEU is the minimum eutectic temperature. Tellerium is observed to decrease secondary dendrite arm spacing, an effect which causes a high carbon equivalent iron like a low carbon equivalent iron with respect to secondary dendrite arm spacing. This demonstrates that Te affects the growth of austenite dendrites prior to its effect on eutectic solidification.[28]

2.5.2 Cellular Structure

The most important fact to recognize regarding cell structure is that it develops after the precipitation of austenite dendrites. Thus cell growth conforms to and superimposed on a dendritic structure that solidifies hosts the cells and therefore can have a major effect on cell nucleation and growth.[23]

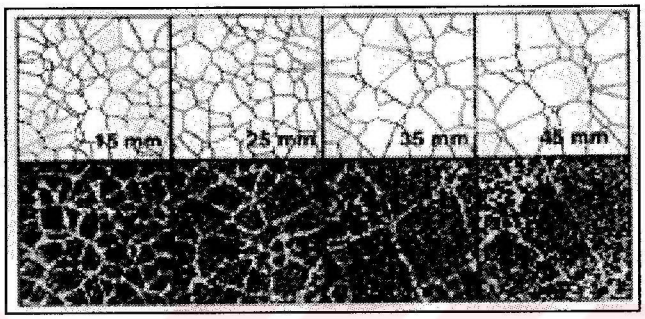

Figure 9. Eutectic cells observed in cast irons

Eutectic cell structure equivalent to that of gray iron is not observed in white iron solidifying with the carbide eutectic. If the Si content is high and the metastable carbide decomposes partially or completely to Type D graphite during solidification no cell structure will be expected. An iron solidifying completely with Type D graphite does not exhibit the typical gray iron cell structure when the eutectic arrest is 1130 °C or below, regardless of whether the iron is hypoeutectic or hypereutectic. This is basic to the Fe-C eutectic solidification process.[28] It should also be mentioned that cell count increases by increasing supercooling. However, gray to white solidification transition in cast iron limits this possibilty.[21]

When the carbon content is very low, coarse interdendritic flake graphite can grow by the columnar mode at eutectic arrest temperatures below 1120 °C. This is also accompanied by the complete absence of eutectic cells in the microstructure. The true eutectic cells may begin to form at any temperature below about 1150 °C and down to about 1130 °C. Eutectic carbide, however, appears to grow only by the columnar, non-cell mechanism.[16]

2.5.3 Graphite

Today it is well realized that the ordinary gray and white structures of cast iron are both the direct result of the solidification reaction. However, it has been suggested many times in the past that the gray structure would be the result of a solid state graphitization process occuring after an initial white solidification reaction. This hypothesis initated several detailed examinations of the solidification reactions around 1950 and very strong evidence was produced to show that hypothesis was wrong. As a consequence, it is now generally agreed that the ordinary flake graphite structure is formed directly from the melt.[15]

The cast iron alloys demonstrate a range of graphite morphologies which start with flake graphite and extend to a graphite form in the shape of a spherulite. Between these two structures, an intermediate form grows referred to as compacted graphite.

These three graphite forms have relatively complex growth mechanisms based on defects in the graphite cyrstal. The flake form grows lengthwise from a rotation boundary and thickens from an array of screw dislocations.

The spherulite grows from a pyramidal form initiating from a screw dislocation and achieves a spherical geometry by repeated faulting. The interface initially takes on the appearance of facets. The compact form retains the growth characteristics of a flake and grows from both a rotation boundary and screw dislocations. Pyramids grow from bounding facets and become unstable giving a type of flake geometry with proturberances of a variety of shapes.[29]

There is a progression in graphite structures as the amount of undercooling increases. Solidification high in the eutectic range results in Type A graphite. Slight amounts of undercooling lead to Type B or rosette graphite. Undercooling to lower temperatures leads to progressively more Types D and E graphite in the microstructure. This is often accompanied by the formation of ferrite as the iron transforms from austenite in the temperature range of about 730 – 790 °C. Severe eutectic undercooling during solidification leads to massive carbide formation and low tensile strengths at undesirably high hardness values.[17]

Like the cell structure, the type of graphite formed during solidification is affected by prior dendrite precipitation and growth. Graphite may nucleate at one or more sites on the solid austenite, compromising the dendritic maze in hypoeutectic irons. Whether the graphite type is Type A or Type D depends on the dendritic growth through the eutectic range. Solidification high in the eutectic range results in coarse dendrite and Type A graphite. Solidification in lower section of the eutectic range causes interdendritic Type D graphite. It has been reported[17] that Type D graphite can bind the matrix to the dendrite fibers tighter than Type A graphite. Hence, a structure consisting of long, oriented and compacted dendrites associated with Type D graphite will have a maximum of strength. Therefore, dendrite morphology, not graphite morphology, is the principal factor determinig strength in irons with similar matrices and compositions.[17]

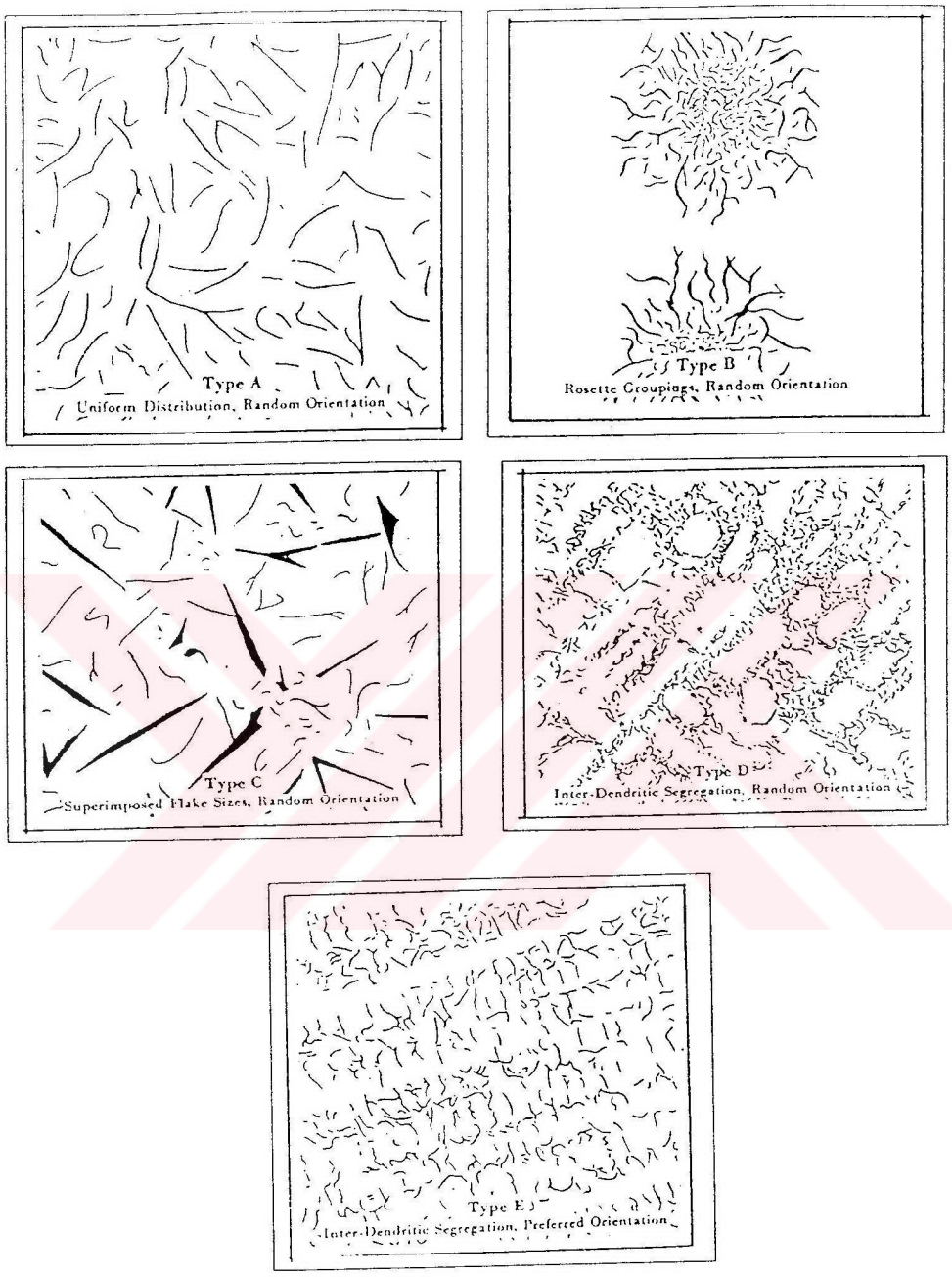

Figure 10. A, B, C, D and E type flakes in gray cast iron

2.5.4 Influence of Sulphur on Graphite Shape

The importance of sulphur has repeatedly been recognized by investigators, studying its effect upon structure. Its coarsening effect on graphite flakes indicated that it reduces the growth rate of the eutectic, but it also greatly increases the degree of nucleation. Cooling curves of specimens with high sulphur content exhibit high undercoolings which is a direct consequence of decreased eutectic growth rate.[30]

In alloys containing sulphur, this element will be enriched at the growing interface as the equilibrium distribution coefficient of sulphur in iron is low (k_o = 0.02). No exact values are known for the distribution coefficient of sulphur in graphite, but it seems to be near unity. However, as the iron and carbon lamellae are growing very closely side by side, the sulphur rejected by the iron will lead to a high sulphur concentration at the interface in general, which can be expected to slow down the diffusion of carbon as well as that of iron and hence decrease the growth rate of both the graphite and austenite phase. Furthermore, sulphur will influence the growth kinetics of the phases, the contact angles, and the interfacial energies between graphite, austenite and the melt respectively. In addition, sulphur decreases the eutectic temperature and the solubility of carbon.[7]

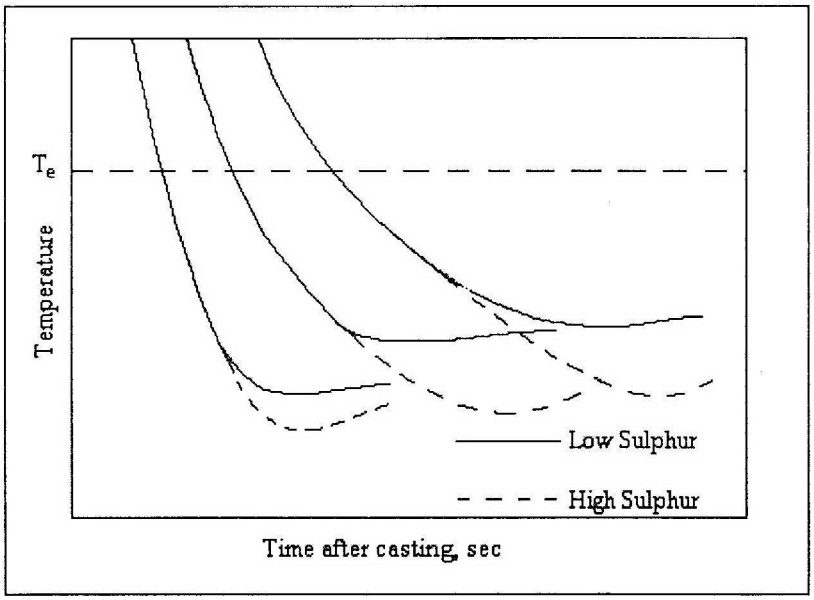

Fig. 11. Effect of sulphur content on undercooling

2.5.5 Mechanical Properties of Gray Cast Iron

Several properties of cast iron are of interest to operating foundrymen, including UTS, fracture toughness, and hardness. These properties are influenced mainly by chemical composition and microstructural features including graphite type, graphite content, matrix microconstitutients and cell count. As most foundry metallurgists know, the composition of the cast iron determines the quantity and character of the graphite, as well as the metallurgical characteristics of the metallic matrix for some specified set of cooling conditions.[23]

Carbide formation is the principal factor which decreases the tensile strength of gray cast iron. Higher carbon equivalent values result in more carbon precipitated during solidification, less matrix continuity and, hence, lower strength values. Conversely, lower carbon equivalent values result in more primary austenite, reduced carbon precipitation during eutectic

solidification, higher matrix continuity, and higher tensile strength values. The strength of cast iron can be easily increased by simply reducing the carbon equivalent, but associated with a reduced carbon equivalent comes an increased tendency for massive carbide formation and chilled edges on castings, which can create machining problems. The most economical method of minimizing the risk of carbide formation in castings is to adjust properly the composition of the iron and add a suitable inoculant to the metal before it is poured. The introduction of a good inoculant provides a large number of nuclei on which graphite can precipitate and grow.[17]

2.6 Thermal Analysis of Gray Cast Iron

2.6.1 Thermal Analysis

Thermal analysis is the process of determining the temperature at which phase transformation - a change in the atomic arrangement - takes place, by observing the aberrations that changes in heat content impose on the rate of temperature change of the specimen.[32]

The ability to measure changes in the solidification process was essential to accomplish the objective of relating such changes to processing variables that commonly occur in foundries, such as variation in chemical analysis, charge materials, superheating temperature and time at temperature, oxidizing melt conditions, melt additions and others. Thermal analysis has the potential capability of measuring the course of solidification processes as well as changes in the processes. Soldification process parameters identified and measured by thermal analysis may then be used to evaluate the effects of processing variables on solidification.[33]

2.6.2 Review of Thermoanalytical Techniques

Thermal analysis may be classified into three major groups based on the parameters measured, namely, energy changes, dimension changes, and weight changes. Among these clasifications, the one which is based on energy changes seems to be the one most widely used, perhaps because more information can be gained from these techniques. Thermal analysis based on energy changes is further divided into three different techniques which are:

1) Cooling or Heating Curve (Temperature vs. Time Plot)
   a) Derived Cooling (heating) Curve, (also called differential curve)
   b) Inverse Rate Curve

2) Differential Scanning Calorimetry

3) Differential Thermal Analysis (DTA)

Cooling curve techniques have been used for a long time as an indirect thermal analysis for carbon equivalent of cast iron melts. Although all information concerning solidification processes is contained in the cooling curve, the only parameters which presently are measured quantatively are phase change temperatures and time. Other solification characteristics are based mostly on qualitative conclusions.[33]

2.6.3 The Energy Equation

The energy equation for an alloy undergoing solidification can be expressed by

$$\rho.C_p.\partial T/\partial t = \nabla\cdot(K\nabla T) + \rho.G \qquad (6)$$

where ρ is the density, C_p is the specific heat, K is the thermal conductivity, and G is the rate of energy generation owing to solidification. It is commonly assumed that latent heat is released at a rate proportional to the rate of formation of the solid fraction, f_s, in castings. Hence, G can be expressed by

$$G = L\,.\,\partial f_s/\partial t \qquad (7)$$

where L is the total latent heat release during solidification.[34]

2.6.4 Methods of Latent Heat Calculation

During phase transformations upon cooling, latent heat is released. This affects the temperature field, which in turn, influences the microstructural evolution.[24] If the enthalpy method is to be used to calculate latent heat, the above energy equation can be combined to become

$$\rho.\partial H/\partial t = \nabla.(K\nabla T) \qquad (8)$$

where H is the enthalpy of the alloy, which is defined by

$$H = \int C_p.dt + L.(1 - f_s) \qquad (9)$$

On the right hand side of Eqn.(9), the first term represent sensible heat, while the second term is the latent heat. If the modified specific heat method is to be employed, by combining Eqns.(6) and (7), the governing equation becomes

$$\rho.C_p^*.\partial T/\partial t = \nabla.(K\nabla T) \qquad (10)$$

where C_p^* is the modified specific heat including both sensible heat and latent heat, and which is defined by

$$C_p^* = C_p - L.\partial f_s/\partial T \qquad (11)$$

It is seen that in order to include latent heat effects, in either the enthalpy method, or modified specific heat method, a relationship between the casting temperature and the solid fraction must be provided. The most simplest and the most widely used relationship is obtained by assuming that latent heat is released linearly between the liquidus temperature, T_l, and the solidus temperature, T_s, which yields

$$f_s = T_l - T \,/\, T_l - T_s \qquad (12)$$

Another mode of latent heat release was proposed by assuming that latent heat is released quadratically between the liquidus and solidus temperatures so that the formulation is given by

$$f_s = 1 - [T - T_s \,/\, T_l - T_s]^2 \qquad (13)$$

Assuming that the solidification process occurs very slowly, such that a complete equilibrium between the solid and liquid phases is established, yields the lever rule

$$f_s = (1 / 1 - p).[T - T_l / T - T_f] \quad (14)$$

where T_f is the fusion temperature of the corresponding pure base metal and p is the equilibrium partition ratio. For a binary alloy, if the liquidus and solidus lines in the phase diagram are assumed straight, then p is constant and can be expressed by

$$p = T_f - T_l / T_f - T_s \quad (15)$$

A fourth mode of latent heat release is obtained by assuming an infinite diffusion in the liquid phase and no diffusion in the solid phase, which yields the well known Scheil equation

$$f_s = 1 - [T - T_f / T_l - T_f]^{1/p-1} \qquad T_e < T \leq T_l \quad (16a)$$

$$f_s = 1 \qquad T = T_e \quad (16b)$$

where T_e is the eutectic temperature of the alloy. The above Scheil equation assumes that the alloy releases latent heat according to the formulation given in Eqn. (16a) above the eutectic temperature, and then the remainder of the latent heat is released at the eutectic temperature which is similar to the case of a pure substance.

The linear and quadratic modes of latent heat release are based purely on assumptions, while the lever rule and Scheil equation are derived under highly simplified conditions. The availability of experimental data relating the solid fraction to casting temperature is very limited. In fact, in many systems it would be difficult, if not impossible, to make a distinction, theoretically or experimentally, between the solid phase and the liquid phase when an alloy is in the mushy condition.[34]

2.6.5 The Lump Heat Method

A modified version of the above represent techniques is the lump heat method, which differs from the others in its pratical approach to handling of latent heat. A lumped system heat balance of the solidification and cooling of the specimen during thermal analysis yields:

$$-h.A.(T - T_{\infty}) + g(t).V = \rho.C_p.V.dT/dt \qquad (17)$$

where T is the temperatrue, t is time, h is the effective heat transfer coefficient for the system, T_{∞} is the ambient temperature, ρ is density, C_p is specific heat, A is the external surface area over which heat extraction occurs, g(t) is heat generation function and V is the volume of the thermal analysis cup .Rearranging equation (17) gives:

$$g(t) = \rho.C_p.[dT/dt + \theta.(T - T_{\infty})] \qquad (18)$$

where θ is the Newtonian cooling parameter defined by:

$$\theta = h.A / \rho.C_p.V \qquad (19)$$

The form of lumped system or Newtonian analysis of raw cooling curve data to calculate latent heats associated with cast iron solidification, a calculation which in effect amounts to integrating the heat generation function, g(t), over the range of solidification, that is;

$$\rho.L = \int g(t)dt \qquad (20)$$

where L is the latent heat of fusion per unit mass.[35]

2.6.6 Thermal Analysis by Interpretation on Cooling Curves

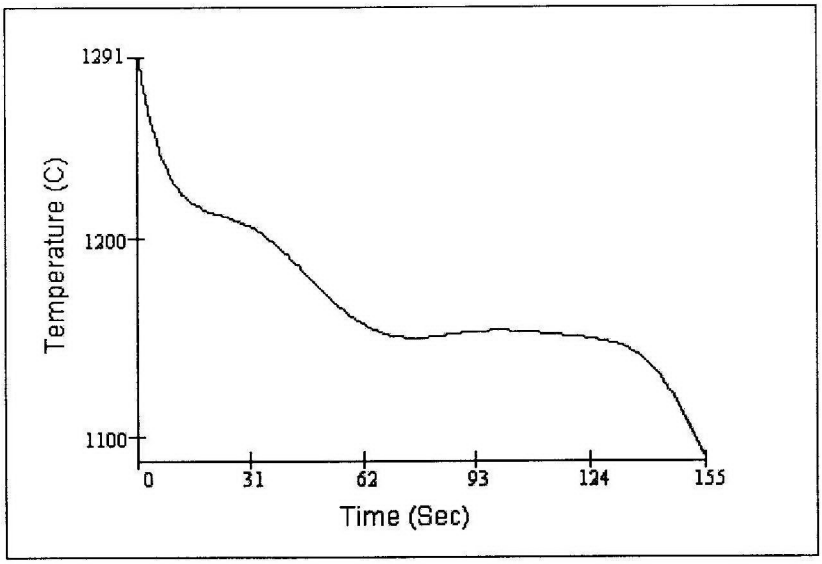

(a)

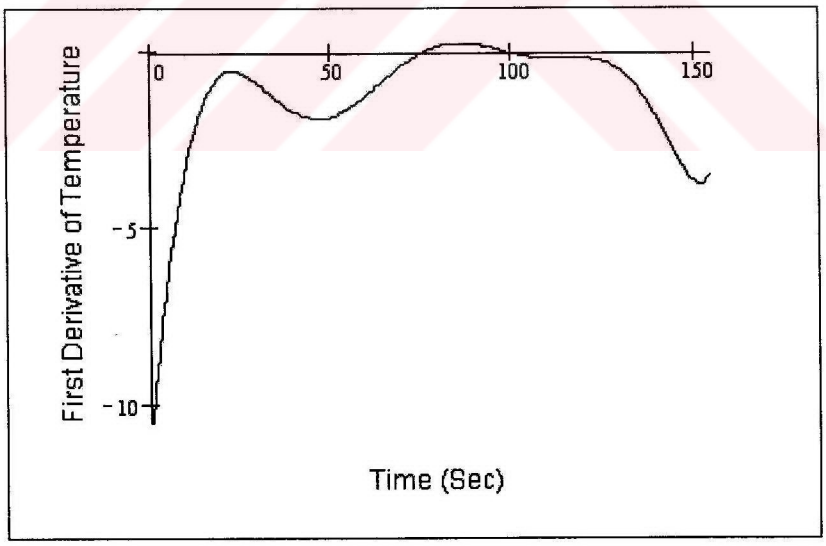

(b)

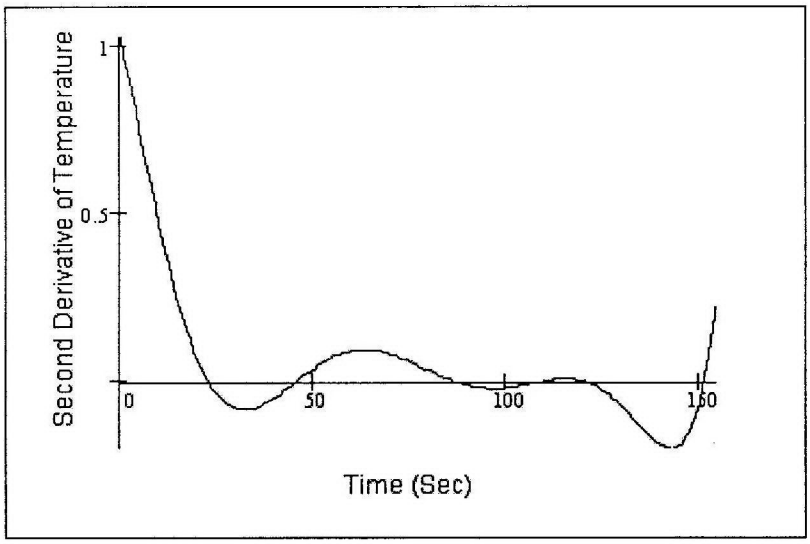

(c)

Figure 12. (a) The cooling curve, (b) the first derivative of the cooling curve and (c) the second derivative of the cooling curve for heat no 31.

It is the evolution of structure through the process of nucleation and growth which will basically determine the form of the cooling curve.[29] The cooling curve in a given heat transfer sysytem results from the sequence of events which occur during the solidification process. Changes in the kind and magnitude of the solidification events during freezing produces changes in the cooling curve. The principle suggests that the cooling curve might be a measure and predictor of the kind macrostructure and microstructure generated during solidification. If true, as cast metallographic structure can then be estimated directly from cooling curves with the potential benefit of predicting the related structures in commercial castings.[28]

Thermal analysis by interpretation of cooling curves has been used in the past, essentially since the end of sixties, to forecast the chemical composition of the molten melt (carbon and silicon contents). The

continuous use of the technique allowed the conclusion to be drawn that the cooling curves contained a lot of information related to the solidification behaviour, as they express the heat balance between the heat released by the molten metal (latent heat and sensible heat) and the heat absorbed by the environment. Thus from thereon, the analysis of the shape of the cooling curves (critical points and other singularities) has been applied to the prediction of the type of cast iron to be obtained after pouring and of the germination potential of the graphite.[1]

The cooling curves for hypoeutectic iron exhibit a primary liquidus arrest which represents the beginning of proeutectic austenite solidification. All the hypoeutectic gray iron curves exhibit undercooling below the equilibrium temperature of eutectic solidification. The undercooling is followed by recalescence which is the difference between the maximum and minimum eutectic temperatures.[28]

For mildly hypereutectic gray cast irons (CE = 4.26 to 4.60) the primary arrest for the graphite liquidus was not detectable on the cooling curve because the latent heat evolution associated with the solidification of graphite is small. For strongly hypereutectic iron (CE > 4.60) this arrest is very obvious. For mildly hypereutectic compositions, it is likelly that an eutectic initiation arrest (TEN) may be mistaken for an austenite liquidus. Normally, an initiating arrest is considerably longer than an austenite arrest.[32]

All information regarding solidification processes is contained in the cooling curve. However, this information cannot be revealed merely by visual examination of the curve itself. A more complete analysis is possible but requires mathematical analysis of data inherent in the curve.[33]

2.6.7 Mathematical Analysis of Thermal Data

2.6.7.1 Newtonian Heat Transfer Theory

The first step of thermal analysis based on Newtonian heat transfer theory is to plot the $\log_e$ of the relative temperature against time. Relative temperature is a dimensionless variable common in both Fourier and Newtonian theory which is defined by

$$\text{Relative Temperature (Y)} = T - T_o / T_i - T_o \qquad (21)$$

where T is the temperature of the sample at any given instant, T_i is the intial temperature of the sample before cooling, i.e., the peak temperature of the cooling curve, and T_o is the ambient temperature or the temperature which the sample will reach at the end of the cooling process. In the Newtonian type of analysis, the $\log_e$ of the relative temperature when plotted against time can be used to calculate the heat transfer parameters of the system and also to monitor the change in heat transfer characteristics during the course of cooling of the sample.

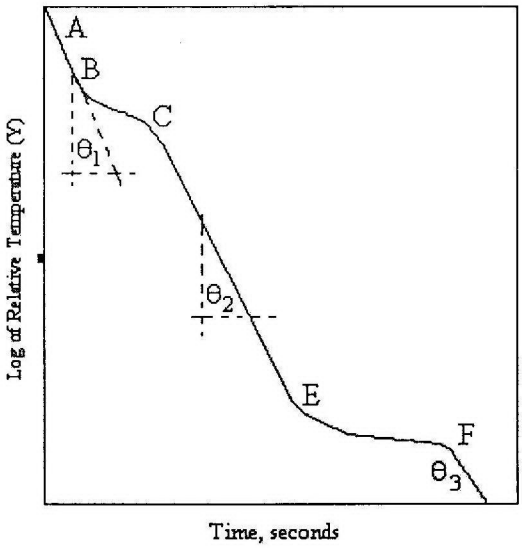

Fig. 13. The heat transfer characteristics curve

The thermal events revealed in Fig. 13 by the Newtonian heat transfer characteristic curve can be summarized as follows:

a) 0 to point A – cooling of the liquid, 0 begins at maximum temperature reached by the thermocouple;

b) Point A – solidification begins at the surface resulting in a changed heat transfer system;

c) A to B – the system is unchanged so the $\log_e$ relative temperature vs. time plot is linear from A to B;

d) B to C – initial growth of austenite at the liquidus displaces the linear portion of the curve until the growth rate of the proeutectic austenite begins to decay exponentially and the relationship of $\log_e$ of relative temperature vs. time again becomes linear;

e) C to E – the linear relationship continues;

f) E to F – heat from eutectic solidification displaces the linear relationship;

g) Below F – the linear relationship of $\log_e$ of relative temperature vs. time is resumed and continues until the eutectoid temperature is reached. After the eutectoid transformation is complete, the linear relationship resumes to near ambient temperature.

Since Newtonian theory applies in the system under study, heat transfer parameters can be determined from the $\log_e$ of relative temperature vs. time curve by using Newton's equation for heat transfer. These heat transfer parameters were used to develop quantitative thermal analysis.[33]

2.6.7.2 The Derivative Curves

The first and second derivatives of the cooling curve is of practical importance in determining the critical temperatures during solidification of the cast iron. Nomenclature and physical meaning of critical points on the cooling curve for hypoeutectic and hypereutectic cast irons are given in tables 2 and 3.

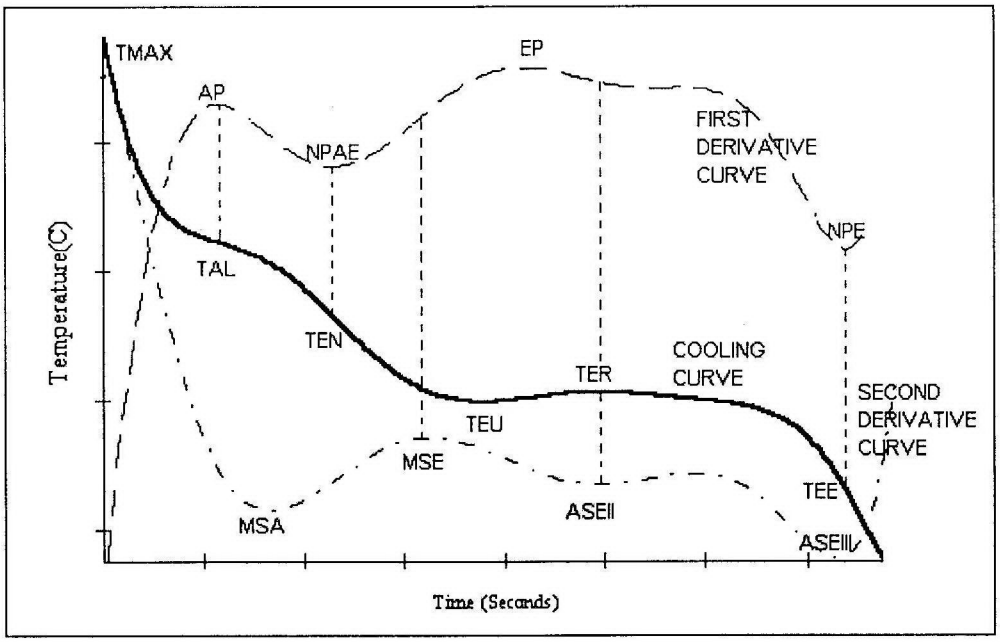

Fig. 14. Cooling curve and its first and second derivative curves for hypoeutectic cast iron, heat no 31.

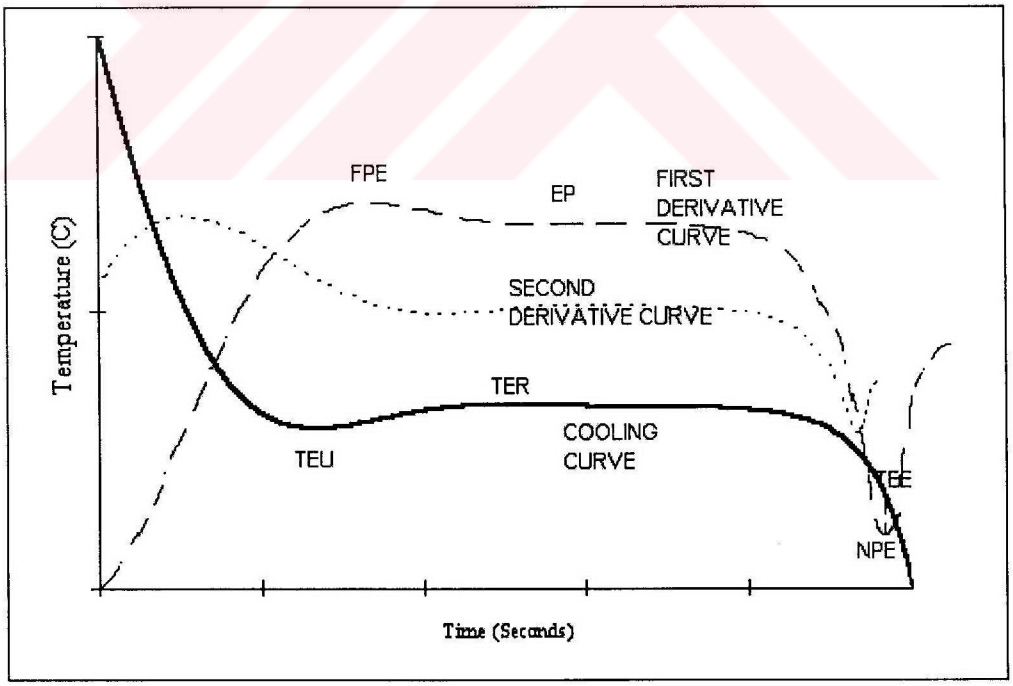

Fig. 15. Cooling curve and its first and second derivative curves for hypereutectic cast iron, heat no 71.

Table 2. Nomenclature and physical meaning of critical points for hypoeutectic cast irons[32]

Curve	Symbol	Nomenclature	Physical Meaning
Cooling curve	TMAX	Maximum temperature	The highest temperature shown on the cooling curve
	TAL	Temperature of liquidus arrest	The temperature at which primary austenite precipitates in hypoeutectic irons
	TEN	Temperature of eutectic nucleation	The temperature at which initial eutectic nucleation occurs and eutectic solidifiacation starts
	TEU	Temperature of eutectic undercooling	The lowest temperature at which the molten iron is undercooled prior to the beginnig of the bulk eutectic growth.
	TER	Temperature of eutectic recalescence	The maximum temperature on the eutectic arrest resulting from the recalescence
	TEE	Temperature of end of eutectic solidification	
First derivative	AP	Austenite peak	The area under this peak is proportional to the amount of proeutectic austenite
	NPAE	Negative peak between austenite and eutectic	The solidification process shifts from austenite to eutectic solidification
	EP	Eutectic peak	The area under this peak is proportional to the amount of eutectic solidified
	NPE	Negative peak after eutectic	The minimum after the eutectic peak corresponding to the end of the eutectic reaction
	SPE	Slope of post eutectic	The portion after the eutectic solidification where no phase transformation occured
Second derivative	MSA	Minimum slope of the austenite peak	The minimum slope of the austenite peak on the first derivative curve
	MSE	Maximum slope of the eutectic peak	The maximum slope of the eutectic peak on the first derivative curve. The duration between MSE and MSA represents the rate of recalescence
	ASE II	Average slope of the eutectic peak in stage II	The average slope of the second stage of the eutectic solidification on the first derivative curve
	ASE III	Average slope of the eutectic peak in stage III	The average slope of the third stage of eutectic solidification on the first derivative curve

Table 3. Nomenclature and Physical Meaning of Critical Points for Hypereutectic Cast Irons[32]

Curve	Symbol	Nomenclature	Physical Meaning
Cooling curve	TMAX	Maximum temperature	See table 2
	TEU	Temperature of eutectic undercooling	See table 2
	TER	Temperature of eutectic recalescence	See table 2
	TEE	Temperature of end of eutectic solidification	
First derivative	FPE	First peak on the eutectic plateau	The first peak on the eutectic plateau of the first derivative curve
	FDE	First discontinuity on theeutectic plateau	The discontiuity preceding FDE on the first derivative curve
	EP	Eutectic plateau	
	NPE	Negative peak after eutectic	See Table 2
	SPE	Slope of post eutectic	See Table 2

Study of the derived cooling curve reveals that no fundamental considerations were involved in the analysis except that the cooling curve data was manipulated such that certain characteristics of the cooling curve could be seen more clearly. Also, no quantitative results in terms of heat of solidification and solidification rate can be obtained from these techniques.

2.6.7.3 Differential Thermal Analysis (DTA)

An improved technique for obtaining more accurate data from a cooling curve uses the computer for differential thermal analysis (DTA). There are two approaches as follows: (i) when temperature measurements are made using this technique experimentally, they are taken with a comparative curve made at the same time for a nontransforming sample; (ii) the computer method constructs a nontransforming curve from the cooling curve using a part of the curve which is transformation free. This replaces the experimentally obtained curve for a neutral reference. Where the part

of the cooling curve with no transformation is small and therefore prone to error in calculation, it can be linearised by calculating a relative temperature vs time curve.[29]

2.6.7.4 The Modified DTA Technique

From the Newtonian heat transfer analysis, it can be seen that the portion of the linear heat transfer curve before and after solidification could represent the heat transfer characteristics of an ideal neutral body for the DTA technique. In other words, if an ideal neutral body were to be found, its thermal properties would be exactly the same as what was calculated from the linear portions of the heat transfer curve mentioned above.

In conventional DTA, the difference in heat evolution between the neutral body and the sample is not measured directly, but the difference in temperature during controlled heating and cooling is measured instead. This temperature differential parameter is later converted into the amount of heat evolved or absorbed with the equations derived for it. So, it is advantageous to proceed directly to calculation of heat evolution instead of measuring the difference in measuring the difference in temperature and later converting to energy evolved. This modified technique then becomes similar to differential calorimetry using the principle of DTA.

The equation derived to calculate the rate of heat given off due to solidification by combining the rate of heat flow from a simulated neutral body and the rate of heat flow from the sample during solidification is given below:

$$q_r / V\rho = c_p [(hA / V\rho c_p)(T - T_o) + dT/dt] \quad (22)$$

where

q_r: rate of heat released by the solidification
V: volume
ρ: density
c_p: specific heat
h: coefficient of heat loss to the surroundings
A: surface area
T: temperature at any given instant
T_o: surrounding temperature

Equation (22) may be written as;

$$q'_r = c_p [\theta(T - T_o) + dT/dt] \quad (23)$$

where

$q'_r = q_r / V\rho$, cal/sec-gm of the sample
$\theta = hA / V\rho c_p$, 1/sec

Note that in Eqn. (23) the rate of heat of reaction is normalized by the mass of the sample. This makes Eqn. (23) become more useful since the mass of the sample is then not involved in the calculation. The parameter θ is the heat transfer parameter calculated from the heat transfer curve (plot of ln relative temperature vs. time) described in the previously. The slope of loge relative temperature vs. time is θ. [33]

There are several primary potential sources of error to evaluate the latent heat of solidification such as the value of the specific heat used in the

calculation of the latent heat. The value used while conducting the calculations in this thesis is 0.108 cal/gm°C.[33] Since the temperature range is close to the melting temperature, the true specific heat is hard to measure, and no data are available. There are discrepancies in the values of the specific heat quoted in different references and the specific heat also varies with different carbon content. Other possible sources of error are as follows:

1) Variation in pouring temperature

2) Variation of the heat transfer coefficient of the sample and sand cup sysytem, due to the tendency of the sand to fall from the walls of the cup as the binder is burned

3) Inconsistency in the amount of iron poured in the cup.[32]

2.6.7.5 Calculation of Percentage of Phases Formed

By knowing the amount of heat released per gram of sample due to solidification, the amount or percentage of phase formed may be calculated provided that the heat of fusion per gram of that phase is known from its thermal property data. For example, let the total heat released at the liquidus arrest be 6.88 cal/g of sample in a gray iron casting. The heat of fusion of austenite from liquid is 65 cal/g of austenite as given in the literature. Then the percentage of austenite formed at the liquidus arrets, ALR, is approximately

% ALR = 6.88 / 65 x 100 cal/gm sample x gm austenite/cal = 10.6%

Thus, the percentage of solids formed at each important stage of solidification can be determined by the modified DTA technique.[33]

CHAPTER 3

EXPERIMENTAL PROCEDURE

3.1 Material and Processing

In the course of this study 14 different gray cast iron alloys of composition shown in Table 4. with carbon equivalent values ranging from 3,30% to 4,56% were produced by casting at various casting temperatures and inoculation percentages. The compositions of the charge materials are given in Table 5. Inoculation is carried out by commercially named SB5 inoculant, which has a composition of 65 – 70 % Si, 1 –1,5 % Al, 1 – 1,5 % Ca, 2 – 2.5 % Ba and remainder Fe.

Table 4. Compositions of the Alloys

Heat No.	% Carbon	% Silicon	CE	% Inoculation
11 – 12	3,64	2,34	4,41	0,8
21 – 22	3,12	1,88	3,75	0,8
31 – 32	3,14	2,50	3,97	0,8
41 – 42	3,21	2,04	3,89	0,8
51 – 52	3,78	2,02	4,45	0,6
61 – 62	3,71	2,56	4,56	0,6
71 – 72	3,39	2,73	4,30	0,6
111 – 112	3,07	1,89	3,70	0,6
121 – 122	2,95	1,95	3,60	0,6

Table 4. Compositions of the Alloys (Continued)

Heat No.	% Carbon	% Silicon	CE	% Inoculation
131 – 132	3,26	1,85	3,88	0,25
141 – 142	3,25	1,91	3,89	0,25
151 – 152	3,22	1,87	3,84	0,25
161 – 162	2,74	3,37	3,86	0,5
171 – 172	2,65	1,96	3,30	0,5

Table 5. Compositon of the Charge Materials

Material	% Carbon	% Silicon
Sorel Metal	4,3	0,2
Steel Scrap	0,2	0,2
FeSi	-	91

Two sand molds, each for casting two bars of dimensions 280 mm in length and 28 mm in diameter were prepared. The standard casting routine consisted of pouring one sample to first sand mold and thermal analysis cup without inoculation, and after inoculating the sample in the furnace, pouring another sample to second sand mold, thermal analysis cup and one sample for spectrometer analysis. Finally, a third sample is poured to thermal analysis cup with tellerium for carbon and silicon analysis.

3.2 Equipment

Ajax Magnethermic coreless induction furnace had been used for melting the prepared charge of the alloys. For achievement of the thermal data from the poured samples, Heraus Electo-Nite Multi-Lab Quik-Cup thermal analysis device is used. Further processing of the thermal data is carried out with MathCad 2000.

Figure 16. Multi-Lab Quik-Cup thermal analysis device

Figure 17. Multi-Lab Quik-Cup and the induction furnaces

Figure 18. Thermal analysis cups, without Te and with Te.

Figure 19. Thermal analysis cups

3.3 Experimental Procedure

3.3.1 Specimen Preparation

3.3.1.1 Metallographic Examination of Specimens

Specimens taken from 4 to 5 cm from one end of prepared bars were used for metallographic examination. The preparation procedure consisted of sandpapering the specimens with 200, 320, 500, 800 and 1200 grid sandpapers, polishing with alumina of 1 micron particle size, and etching with 5% Nital for 30 seconds for eutectic cell size and graphite measurements and with amonium oxide per sulphide solution for 30 seconds for dendrite measurements.

3.3.1.2 Tensile Test Specimens

The test is performed on a round, machined test piece in which the middle section of the length is reduced in diameter. The produced bars were machined to following dimensions:

Table 6. Tensile Test Specimen Dimensions

Length:	260 mm
Radius:	18,5 mm
Inner Radius:	12 mm
Reduced Length:	76 mm
Gauge Length:	61 mm

3.3.2 Experiments

3.3.2.1 Chemical Analysis

The chemical analysis of the specimens are carried out in Extra Metal and Erkunt A.Ş. laboratories. Both foundries used OBFL spectrometer for chemical analysis and the results given are average of at least three repetitions.

3.3.2.2 Metallographic Examinations

Six different parameters, which are eutectic cell count (ECC), dendrite secondary arm spacing (DAS), percent dendrite interaction area, graphite flake count, graphite size and graphite type are investigated through metallographic examination.

The cell count was carried out by the line intercept method. After drawing a line across the diameter of the sample, the number of cells intersecting 1 cm of this diameter were counted and the number of cells per cm obtained. This number, converted to the number of cells per cm^2 was used as the cell count. The cell count values reported here are average of three repetitions. The cell count was performed with Olymus optical microscope at a magnification of 10X.

For secondary dendrite arm spacing and dendrite interaction area measurements the metallographic specimens were heat treated to develop ferrite in dendrites for better visual quality. The heat treatment to ferritize the dendrites involved

1. Austenizing the samples for 1 hour at 890 °C
2. Rapidly dropping the temperature to 800 °C
3. Slowly cooling to 650 °C
4. Air cooling.

The specimens were then metallographically polished and etched with $(NH_4)_2S_2O_8$ and examined with Wilson scaled optical microscope at a magnification of 20X. Three fields were examined and the secondary arm spacing of the largest dendrites were then averaged. The dendrite interaction area represents a qualitative estimate of the area fraction of dendrites present in each of three fields.

Wilson scaled optical microscope was used to measure the graphite flake morphology, graphite flake count, maximum major shape axis length and average major axis length at a magnification of 20X. The major shape axis length is defined as the linear distance between the two ends of a graphite flake. The reported values are averaged from three measurements taken from different random areas inside the eutectic cells.

3.3.2.3 Tensile Test

The ultimate tensile strength of the machined specimens were measured in a calibrated Alşa testing machine which has a capacity of 60 tons. The testing machine had a transmitting slidewire to provide an electirical signal proportional to the load applied for digital illustration purpose. Dimensions of a standard tensile test specimen is given in Figure 20.

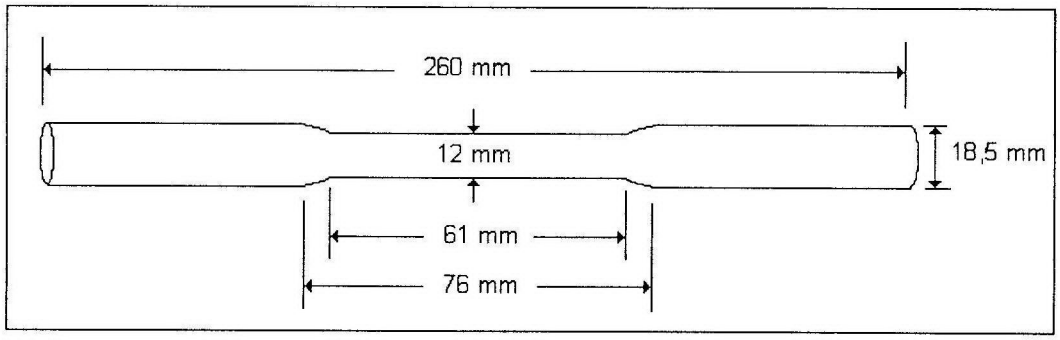

Figure 20. Dimensions of a standard tensile test specimen

3.3.2.4 Thermal Analysis

A program is written in Mathcad to process the thermal data obtained from Multi-Lab Quik-Cup thermal analysis device for plotting the cooling curve, its first and second derivative for calculation of critical temperatures on the cooling curve such as, temperature of austenite liquidus (TAL), temperature of eutectic nucleation (TEN), temperature of eutectic undercooling (TEU), temperature of eutectic recalescence (TER) and temperature of end of eutectic solidification. Further analysis of the data consisted of calculating the log of relative temperature vs time plots for calculation of Newtonian cooling parameter and calculation of rate of heat of solidification at every time step for both primary dendrites and the eutectic.

For illustration purpose of the thermal analysis method, the cooling curve and relative temperature vs time plot for heat no 172 is given below.

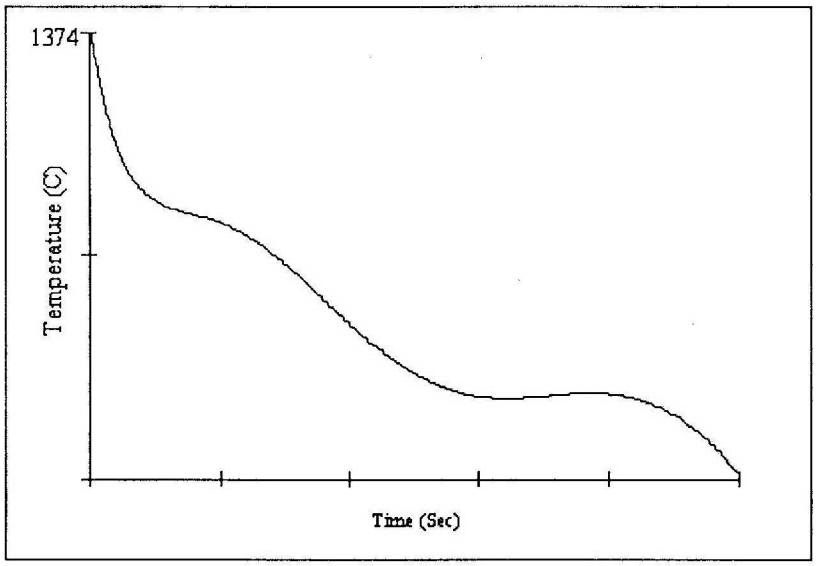

Figure 21. Cooling curve for heat no. 172

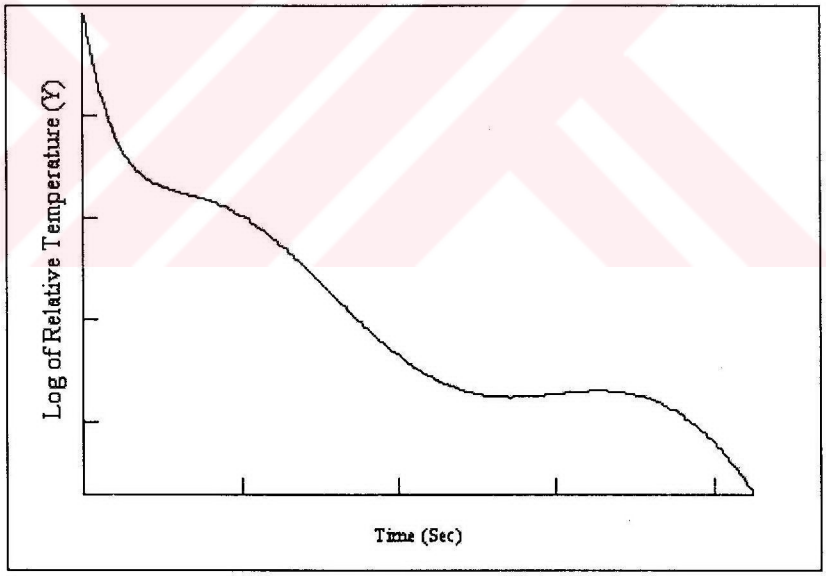

Figure 22. Relative temperature vs time plot for heat no. 172

Table 7. Worksheet for Thermal Analysis of Primary Solidification of Heat No172

Time	T (°F)	dT/dt	LnY x10^{-3}	θ1	θ'	θ2	q_r	t'	S.M.	I
0	2505,3									
1	2348,2	-157,14	-0,065							
2	2342,1	-6,12	-0,068	2,637			-0,028	1		
3	2336,7	-5,4	-0,070	2,333			-0,024	1		
4	2331,8	-4,86	-0,072	2,104			-0,022	1		
5	2327,7	-4,14	-0,074	1,796			-0,018	1		
6	2323,9	-3,78	-0,075	1,642			-0,733	1	0,333	-0,244
7	2320,5	-3,42	-0,077		1,643		0,051	1	1,33	0,068
8	2317,6	-2,88	-0,078		1,613		0,142	1	0,67	0,095
9	2315,1	-2,52	-0,079		1,583		0,198	1	1,33	0,263
10	2312,9	-2,16	-0,080		1,552		0,254	1	0,67	0,170
11	2310,9	-1,98	-0,081		1,522		0,275	1	1,33	0,366
12	2309,1	-1,8	-0,082		1,492		0,296	1	0,67	0,198
13	2309,3	0,18	-0,082		1,462		0,668	1	1,33	0,888
14	2306,3	-3,06	-0,083		1,432		0,025	1	0,67	0,017
15	2305,0	-1,26	-0,084		1,402		0,361	1	1,33	0,480
16	2302,7	-2,34	-0,085		1,371		0,138	1	0,67	0,092
17	2301,8	-0,9	-0,085		1,341		0,404	1	1,33	0,537
18	2300,9	-0,9	-0,086		1,311		0,391	1	0,67	0,261
19	2300,0	-0,9	-0,086		1,281		0,377	1	1,33	0,502
20	2299,1	-0,9	-0,086		1,251		0,364	1	0,67	0,244
21	2298,2	-0,9	-0,087		1,221		0,351	1	1,33	0,467
22	2297,3	-0,9	-0,087		1,119		0,307	1	0,67	0,205
23	2296,4	-0,9	-0,088		1,16		0,324	1	1,33	0,432
24	2295,3	-1,08	-0,088		1,13		0,276	1	0,67	0,185
25	2294,4	-0,9	-0,088		1,1		0,298	1	1,33	0,397
26	2293,3	-1,08	-0,089		1,07		0,250	1	0,67	0,167
27	2292,0	-1,26	-0,089		1,039		0,202	1	1,33	0,268
28	2291,0	-1,08	-0,090		1,009		0,223	1	0,67	0,149
29	2288,3	-1,44	-0,091		0,979		0,140	1	1,33	0,187
30	2286,8	-1,26	-0,091		0,949		0,162	1	0,67	0,108
31	2285,4	-1,44	-0,092		0,919		0,114	1	1,33	0,152
32	2283,8	-1,44	-0,092		0,889		0,101	1	0,67	0,068

Table 7. Worksheet for Thermal Analysis of Primary Solidification of Heat No172 (Continued)

Time	T (°F)	dT/dt	LnY x10^{-3}	θ1	θ'	θ2	q_r	t'	S.M.	I
33	2282,0	-1,62	-0,093		0,858		0,053	1	1,33	0,070
34	2280,2	-1,8	-0,094		0,828		0,004	1	0,67	0,003
35	2278,4	-1,8	-0,095		0,798		-0,008	1	1,33	-0,010
36	2276,6	-1,8	-0,095			0,798	-0,008	1	0,333	
37	2274,8	-1,8	-0,096			0,799	-0,008	1		
38	2272,6	-2,16	-0,097			0,959	-0,009	1		
									Total I = 7,055	

Heat of reaction = 7,055 Btu / lb

= 7,055 x 252 / 454 cal / gm

= 3,916 cal / gm

The table above illustrates the calculation of heat of solidification of primary solidification for heat no 172. The steps of calculation of Table 7 are as follows:

1. The first column represents the time step. The data in the first row is the peak temperature in the cooling curve.
2. The second column is the temperature of the sample converted to °F for the ease of calculations
3. The third column is the first derivative of the cooling curve calculated by numerical differentiation.
4. The fourth column is the relative temperature values at each corresponding time step. The aim of using relative temperature is to establish a linear change of temperature with temperature when to transformation occurs, so that the Newtonian cooling parameter can be calculated by simply calculating the slope of these linear portions.

5. The fifth column is for the calculation of Newtonian cooling parameter θ which is the slope of Ln Y versus time. θ_1 values correspond to the part of the cooling curve before precipitation of austenite.
6. Column six calculates the values of θ' compensated between θ_1 and θ_2 assuming a linear change of θ with time.
7. Column seven lists the values of θ_2 as in column five. θ_2 values correspond to the part of the cooling curve after primary solidification.
8. Column eight represents the rate of heat of solidification at the liquidus arrest by application of Eqn. (23).
9. Columns 9, 10 and 11 are used for numerical integration to obtain the total heat of solidification during time steps t_7 to t_{36}. Simpson's rule of integration will be used which is;

$$f(x)dx = t'/3\ [f(x_0) + 4f(x_1) + 2f(x_2) + 4f(x_3) + \ldots + 4f(x_{n-1}) + f(x_n)]$$

where t' is the time interval between data points, listed in column 9.

In this illustration, t' is equal to 1 second. The Simpson Multipliers of 1/3, 4/3, 2/3, 4/3, . . ., 2/3, 4/3, 1/3 are set in column 10 between time intervals t_7 and t_{36}. Column 11 is the calculation of partial terms by Simpson's method of numerical integration. The sum of all values in column 11 is the solution of this integration which is defined as the total heat of solidification.

CHAPTER 4

EXPERIMENTAL RESULTS AND DISCUSSION

4.1 Experimental Results

Solidification parameters of gray cast iron are examined and correlation of these parameters to cooling curve variables is conducted through thermal analysis by interpretation of cooling curves.

4.1.1 Chemical Analysis Results

The results of the spectrometer analysis are given in the table below.

Table 8. Chemical Analysis Results

No	C	Si	Mn	P	S	Mg	Cr	Ni
12	3,64	2,30	0,024	0,026	0,004	<0,001	0,019	0,005
22	3,12	1,88	0,043	0,021	0,006	<0,001	0,008	0,007
32	3,14	2,50	0,248	0,030	0,035	<0,001	0,009	0,041
42	3,21	2,04	0,065	0,024	0,011	<0,001	0,019	0,006
52	3,78	2,02	0,042	0,021	0,012	<0,001	0,013	0,002
62	3,71	2,55	0,042	0,027	0,007	<0,001	0,016	<0,001
72	3,39	2,73	0,055	0,032	0,010	<0,001	0,024	0,014
112	3,07	1,89	0,081	0,027	0,010	<0,001	0,026	0,019
122	2,95	1,95	0,093	0,023	0,009	<0,001	0,026	0,018
132	3,26	1,85	0,710	0,035	0,061	<0,001	0,057	0,024
142	3,25	1,91	0,725	0,040	0,059	<0,001	0,053	0,022
152	3,22	1,87	0,712	0,034	0,057	<0,001	0,076	0,025
162	2,74	3,37	0,117	0,036	0,015	<0,001	0,007	0,001
172	2,65	1,96	0,078	0,025	0,011	<0,001	0,026	0,031

4.1.2 Metallographic Examination Results

The first part of the measurements consisted of eutectic cell count (ECC), secondary dendrite arm spacing (DAS) and percent dendrite interaction area (%Int). As mentioned earlier, the dendrite interaction area represents a qualitative estimate of the area fraction of the dendrites rather then a quantiative numerical calculation.The results are given in the table below.

Table 9. Results of Metallographic Examination, Part 1

Heat No.	ECC (cell/cm^2)	DAS (μm)	%Int
11	196	No dendrites	No dendrites
12	841	No dendrites	No dendrites
21	400	30	90
22	1156	15	40
31	596	45	80
32	1369	25	60
41	400	35	70
42	961	25	60
51	361	No dendrites	No dendrites
52	1156	No dendrites	No dendrites
61	324	No dendrites	No dendrites
62	1225	No dendrites	No dendrites
71	256	No dendrites	No dendrites
72	1681	No dendrites	No dendrites
111	729	40	90
112	1681	10	40
121	256	35	70
122	2025	30	70
131	441	20	80
132	1681	30	80
141	529	40	100
142	1296	30	100
151	324	12	100
152	841	15	80
161	289	50	70
162	441	40	10
172	1681	25	80

The second part of the metallographic measurements involved examination of graphite. Graphite flake count, maximum major shape axis length, average major shape axis length and graphite type are investigated through metallographic examination. The major shape axis length is defined as the linear distance between the two ends of a graphite flake. The results are given in the table below.

Table 10. Results of Metallographic Examination, Part 2

Heat No.	Graphite Count	Average Length (μm)	Maximum Length (μm)	Type
11	172	55	220	A
12	142	110	400	A
21	142	40	220	A
22	60	80	190	A
31	78	65	180	A, D
32	192	85	190	A
41	208	80	240	A
42	90	75	200	A
51	116	70	160	A
52	114	86	170	A
61	210	123 (C)	280 (C)	D, C
62	92	80	240	A, C
71	216	25	180	C
72	169	77	350	C
111	206	55	205	A
112	94	85	150	A
121	96	65	200	A
122	118	55	250	A
131	186	150	35	D, A
132	52	77	150	A
141	84 (A)	50 (A)	230 (A)	D, A
142	326	25	100	E
151	78	75	215	D, A
152	142	55	115	A
161	122	95	190	A
162	94	65	200	A
172	412	45	120	D, E

4.1.3 Tensile Test Results

The results of the tensile tests are given in the table below.

Table 11. Tensile Test Results

Heat No	UTS (MPa)	Heat No.	UTS (MPa)
11	103,2	111	240,0
12	113,2	112	272,0
21	274,0	121	273,6
22	287,2	122	310,0
31	291,2	131	232,0
32	260,4	132	299,6
41	246,8	141	254,4
42	306,0	142	284,0
51	175,6	151	249,6
52	206,8	152	280,0
61	118,0	161	224,0
62	135,2	162	229,2
71	149,6	172	272,0
72	138,4		

4.1.4 Thermal Analysis Results

4.1.4.1 Critical Temperatures on Cooling Curves

Peak temperature on the cooling curve, temperature of austenite liquidus (TAL), temperature of eutectic nucleation (TEN), temperature of eutectic nucleation (TEN), temperature of eutectic recalescence (TER), temperature of end of eutectic solidification (TEE) and undercooling (ΔT) values are given in the table below.

Table 12. Critical Temperatures on Cooling Curves

Heat No.	Peak (°C)	TAL (°C)	TEN (°C)	TEU (°C)	TER (°C)	TEE (°C)	ΔT (°C)
11	1370,0	-	X	1141,4	1151,9	1137,8	10,5
12	1370,0	-	X	1149,7	1155,8	X	6,1
21	1339,3	1216,4	1182,4	1146,0	1151,5	X	5,5
22	1285,0	1223,1	1195,6	1153,2	1155,9	X	2,7
31	1290,3	1211,3	1181,6	1149,8	1153,5	1102,9	3,7
32	1306,9	1203,7	1178,4	1152,4	1155,4	994,6	3,0
41	1344,7	1207,1	1176,2	1145,4	1149,8	1097,1	4,4
42	1370,0	1208,5	1179,0	1149,8	1154,9	X	5,1
51	1346,2	-	1160,1	1149,8	1155,5	X	5,7
52	1370,0	-	1163,0	1151,1	1157,0	X	5,9
61	1350,9	-	1162,2	1148,9	1163	X	14,1
62	1312,9	-	X	1155,8	1162,2	X	7,0
71	1305,7	-	X	1145,9	1155,4	X	9,5
72	1370,0	-	X	1149,5	1158,6	X	9,1
111	1313,2	1219,9	1188,9	1147,3	1151,7	X	4,4
112	1255,9	1225,4	1191,4	1150,8	1154,4	X	3,6
121	1341,8	1226,0	1187,6	1144,7	1149,1	X	4,4
122	1332,2	1228,6	1195,0	1152,0	1153,4	X	1,4
131	1320,8	1213,5	1181,8	1128,9	1134,4	X	5,5
132	1318,3	1213,1	1180,7	1142,4	1147,8	X	5,4
141	1321,9	1198,1	1166,5	1131,8	1137,6	X	5,8
142	1329,1	1200,8	1171,9	1141,9	1146,8	X	5,5
151	1336,2	1200,2	1169,9	1130,3	1137,2	X	6,9
152	1323,7	1199,9	1171,0	1141,7	1147,2	X	5,5
161	1370,0	1199,1	1174,6	1150,1	1157,4	X	7,3
162	1300,3	1208,3	1185,8	1155,5	1157,7	X	2,2
172	1370,0	1259,5	1204,5	1142,7	1146	X	3,3

A mildly hypereutectic cast iron (CE = 4.26 to 4.50%) exhibits a prolonged eutectic initiation arrest. This mainly because the heat of solidification of primary graphite in hypereutectic irons is considerably low so that it does not create any inflection on the cooling curve and as a result, the temperature of graphite liquidus could not be detected in the cooling curves. Also, as a consequence of prolonged eutectic initiation arrest of hypereutectic irons, it is very difficult to detect the temperature of eutectic nucleation (TEN) in these alloys. Other missing values in end of eutectic solidification temperature (TEE) values are because of insufficient temperature range of thermal analysis device.

4.1.4.2 Heats of Solidification and Integral Areas

The calculated values for heat of primary solidification for hypoeutectic alloys and heat of eutectic solidification for hypoeutectic, eutectic and hypereutectic alloys and values A1 and A2 areas are given in the table below. A1 area is defined as the integral area under the cooling curve between TEN and TEU and A2 area is defined as the integral area under the cooling curve between TEN and TER. A relationship between the eutectic cell density and the cooling curve is expected. A1 area represents the range of eutectic nucleation by considering the temperature of interest, rate of temperature and time interval for the eutectic nucleation. TEU is the end of eutectic nucleation but it's thermal effect continues up to TER. Therefore A2 area is also found to be significant in examining an index to the eutectic cell count.

Table 13. Heats of Solidification and Integral Area Values

Heat No	Heat of Primary Solidification (cal / gm)	Heat of Eutectic Solidifation (cal / gm)	A1 area	A2 area
11	-	69,093	X	X
12	-	75,913	X	X
21	2,641	58,408	47480	88850
22	1,956	51,570	65200	102100
31	1,202	51,098	35960	62450
32	1,996	50,817	45260	79890
41	0,645	55,229	42750	72590
42	1,865	54,804	55660	96000
51	-	44,393	40370	87640
52	-	39,587	46200	92380
61	-	49,056	19600	93560
62	-	76,642	X	X
71	-	88,238	X	X
72	-	118,096	X	X
111	3,492	50,477	52240	92480
112	1,075	52,962	44230	78810
121	1,088	63,294	47510	91110
122	1,856	44,811	55240	103200
131	2,255	46,026	81470	124500
132	0,710	71,331	61230	108200
141	1,071	62,368	53740	110500
142	1,660	50,679	55270	113700
151	0,711	TC Break	67450	110500
152	2,264	47,934	54110	105600
161	1,474	41,792	44010	89030
162	1,637	44,570	58220	92540
172	3,916	54,811	69800	10300

Because solidification of eutectic alloys start with eutectic solidification and hypereutectic alloys start with precipitation of primary graphite, which has a very small heat of solidification compared to primary austenite solidification, the heat of primary solidification values are not present for these alloys. Moreover, absence of TEN values for these alloys make it impossible to calculate A1 and A2 areas, so values for these alloys could not be given in the table above.

4.2 Discussion of Results

4.2.1 Effect of Macrostructure on Strength of Cast Iron

In early published papers, eutectic cells have always been emphasized in relationship with mechanical properties of cast iron. In all investigations, however, where also the primary structure, which is the dendritic structure formed at the liquidus arres, has been examined, it was shown that the effect of primary structure exceeds that of eutectic cells. Highest tensile strengths are obtained with large denrites and higher interaction areas, lowest tensile strengths are obtained when the denrites are short and weak in interaction. As an extreme case, Glover et al.[17] were not able to find any significant statistical relation ship between ECC and tensile strength.

These statements are in accordance with the results of the present research. Secondary dendrite arm spacing and dendrite interaction area are found to be the most important two parameters in determining the strength of gray cast iron. Eutectic cell count also plays a significant role, but its importance takes place after denrite parameters.

With application of a multiple linear regression equation in order to correlate tensile strength (TS) values with secondary dendrite arm spacing (DAS), percent dendrite interaction area (%Int) and eutectic cell count (ECC), the following equation, with a correlation coefficient (R2) value of 0,47 is obtained:

$$TS = 69,97 - 0,287(DAS) + 1,74(\%Int) + 0,059(ECC) \qquad (24)$$

By potential application of the above equation, tensile strength values can be predicted with putting the appropriate DAS, %Int and ECC values. For example, ECC is 1681, DAS is 30 and %Int value is 80 for heat no. 132. Putting these values in above equation yields:

$$TS = 69,97 - 0,287(30) + 1,74(80) + 0,059(1681)$$

yields a tensile strength value of 299,7 MPa, where the actaul measured value is 299,6 MPa, which is very close to the calculated value.

4.2.2 Effect of Composition on Strength of Cast Iron

The most important result regarding the importance laid on denrites in relationship with strength of cast irons arises when tensile strength values of eutectic and hypereutectic alloys are considered. Despite their high eutectic cell count, because these alloys solidify without precipitation of austenite denrites, their tensile strength values are approximately half of the hypoeutectic alloys.

A relationship exists between the carbon equivalent of cast iron and tensile strength. Higher carbon equivalent values result in more carbon precipitated during solidification and hence, lower strength values. Conversely, lower carbon equivalents result in more primary austenite, reduced carbon precipitation during eutectic solidification and higher tensile strength values. Figure 23 shows effect of carbon equivalent on tensile strength.

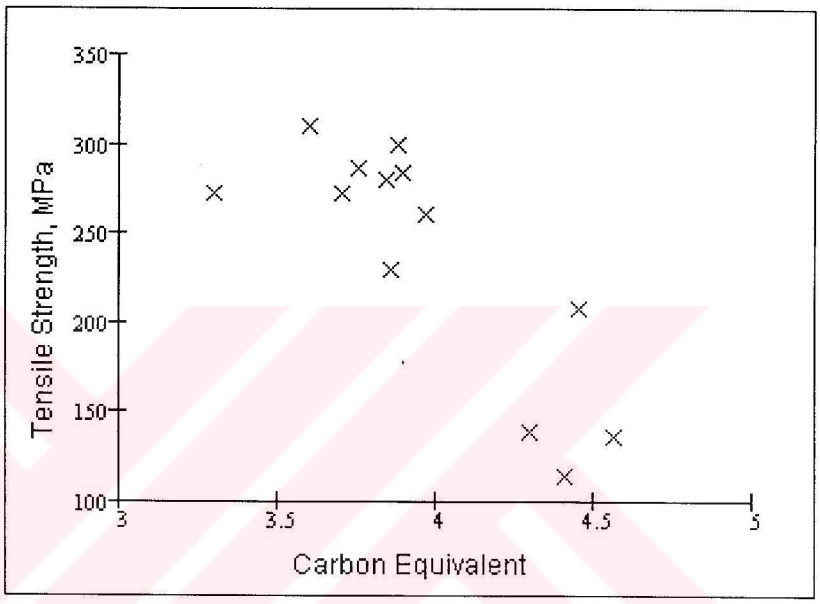

Figure 23. Effect of CE on tensile strength

For the ease of understanding the effect of carbon equivalent on tensile strength, the best line fitting to data in Figure 23 is calculated by regression analysis which yields the following equation;

$$TS = 855{,}15 - 154{,}56(CE) \qquad (25)$$

in which value of (R2) is 0,67. From this equation it can be concluded that tensile strength decreases with increasing carbon equivalent.

4.2.3 Graphite Formation in Gray Cast Iron

It has been stated in the literature (17) that there is a progression in graphite structures as the amount of undercooling increases. Undercooling high in the eutectic range results in type A graphite and progression proceeds to type B, C, D and finally to type E as the undercooling further increases. However, the results obtained in present work are not consistent with this statement. Some alloys solidifed at minimum eutectic temperature values of 1155.5 – 1142,4 °C contained type A graphite, type C graphite precipitated in some alloys regardless of the range of eutectic temperature, but type D and E graphites are always associated with lower (1148,9 – 1130,3) minimum eutectic temperatures.

A more consistent result arises when the carbon equivalent values are considered. There are exceptions, but the general tendency is in the way that as the carbon equivalent of the cast iron increases, the progression in graphite types proceed from type A to type C and D.

It is quite hard to establish a direct relationship between graphite types and only one parameter, such as carbon equivalent or minimum eutectic temperature. From the literature review, in all actions undertaken to influence graphite formation also change the primary structure and as a consequence this primary phase force the graphite to change its dimension, distribution and shape. This could lead to the conclusion that, the graphite type formed in a cast iron is not a direct result of the effect of carbon equivalent or minimum eutectic temperature but combination of many parameters that affect the whole solidification process.

4.2.4 Interpretation of Cooling Curves

Solidification of hypoeutectic gray cast iron starts with precipitation of primary austenite dendrites and the heat of primary solidification associated with solidification of these primary dendrites create an inflection on the cooling curve, which is reffered to as temperature of austenite liquidus. The effect of composition on the temperature of astenite liquidus (TAL) is investigated and the following regression equation is obtained;

$$TAL = 1263 - 13{,}58.(CE) \qquad (26)$$

with an (R2) value of 0,063. The correlation coefficient is very low, so it yields almost no statistical significance. In order to obtain a better definiton of temperature of austenite liquidus in terms of composition, the temperature in consideration had been subjected to a more detailed regression analysis by considering all elements that exhibit large deviations in chemical analysis. The following regression equation seems to be much more significant;

$$TAL = 1218{,}07 + 5{,}23.(CE) + 154{,}9.(\%S) - 979{,}17.(\%P) - 11{,}24.(\%Mn) \qquad (27)$$

with a (R2) value of 0,51. The depressing effect of phosphorus is interestingly very dominant and sulphur has a slight effect of increasing the temperature of austenite liquidus. By knowing the strong effect of phosphorus, the effect of carbon equivalent liquidus (CEL) on temperature of austenite liquidus and there found to be a very strong relationship with an (R2) value of 0,90.

$$TAL = 1541{,}5 - 89{,}9.(CEL) \qquad (28)$$

It has been known that there exists a clear relationship between carbon equivalent, amount of inoculation and the minimum eutectic temperature (TEN), which is also verified by the result of present research. The corresponding regression equation is;

$$TEU = 1112,5 + 6,58.(CE) + 21,3.(\%Inoc) \quad (29)$$

with an (R2) value of 0,75 which means that the above equation is considerably reliable.

Another relationship could also be established between carbon equivalent, amount of inoculation and eutectic recalescence. The governing regression equation is;

$$\Delta T = -4,62 + 2,66.(CE) - 3,19.(\%Inoc) \quad (30)$$

with an (R2) value of 0,39 which can also be considered as statistically significant.

When it comes to evaluation of heat of primary solidification and heat of eutectic solidification, no significant relationships could be established between the heat of primary solidification and secondary dendrite arm spacing, and heat of eutectic solidification end eutectic cell count. This result arises from the fact that heats of primary and eutectic solidification indicates the bulk amount of austenite and eutectic formed and do not provide any indication on the number of dendrites or eutectic cells. From this point of view, there expected to be a relationship between the heat of primary solidification and percent interaction area of the dendrites since dendrite interaction may be regarded as an index to amount of bulk austenite precipitated. The calculated relationship is not strong (R2 = 0,03) but reflects the expected result:

Heat of Primary Solidification (cal / gm) = 0,488 + 0,014.(%Int)
(31)

Finally, a correlation between eutectic cell count and A1 and A2 areas had been investigated. The results indicated that A2 area has no relevance with the density of eutectic cells. A1 area has a weak correlation with (R2) value of 0,06 which is given by,

ECC = 313,1 + 0,0105.(A1) (32)

Therefore, the discussion above can be accepted to be valid for A1 and A2 areas, which can be stated as; A1 and A2 areas seem to have very low correlation with the heat of eutectic solidification (R2 = 0,014 for A1 and R2 = 0,00073 for A2), as a consequence with the amount of bulk eutectic solidified, but no relevance with the eutectic cell count.

4.2.5 Interpretation of Thermal Analysis Results

In the literature (36) latent heat of fusion values of austenite and gray cast iron are given as 65 and 55 cal / gm, respectively. As mentioned earlier, by knowing the amount of heat released per gram of sample due to solidification, the amount or percentage of phase formed may be calculated provided that the heat of fusion per gram of that phase is known from its thermal property data. For example, the total heat released at the liquidus arrest is 3,916 cal/gm of sample in heat no 172 as demonstrated previously. The heat of fusion of austenite from liquid is 65 cal/gm of austenite as given in the literature. Then the percentage of austenite formed at the liquidus arrets, ALR, is approximately

% ALR = 3,916 / 65 x 100 = 6,02 %

It should be noticed that this value is valid only for primary solidification of heat no 172. Same argument also applies to eutectic solidification and the calculated values are given in the table below;

Table 14. Percentages of Austenite and Eutectic Solidifed

Heat No.	Percentage of Austenite Solidifed	Percentage of Eutectic Solidified
22	3,01%	93,76%
32	3,07%	92,39%
42	2,87%	99,64%
112	1,65%	96,29%
122	2,86%	81,47%
142	2,55%	92,14%
152	3,48%	87,15%
162	2,52%	81,04%
172	6,02%	99,66%

Only the values of inoculated samples are tabulated since uninoculated samples contain cementite, which has a different latent heat of fusion value (46,6 to 59 cal / gm) than gray cast iron so that calculated percentages would be wrong. Although the latent heat of fusion of gray cast iron is given as 55 cal / gm, values obtained from eutectic and hypereutecic composition exceeded this value, which is physically impossible. This error may be due to difficulties in determining the Newtonian heat transfer parameter during phase transformation. Methodoligies offered in the literature[33] still lack of clarity.

When above tabulated results are considered, there found a more clear relationship between percent austenite solidified at the liquidus arrest and percent dendrite interaction;

$$\% \text{ Int} = 35{,}33 + 8{,}28.\ (\%\text{ALR}) \qquad (33)$$

with (R2) value of 0,16.

No significant relationship could still be established between the percent eutectic solidifed and eutectic cell density, and the percent austenite solidifed and secondary dendrite arm spacing. Therefore, as mentioned previously, those percentage values can only be used as an index to bulk amount of austenite and eutectic solidifed and have no relevance with the number of dendrites or cells.

CHAPTER 5

CONCLUSIONS

1. Secondary dendrite arm spacing and dendrite interaction area are found to be the most important two parameters in determining the strength of gray cast iron. Eutectic cell count also plays a significant role, but its importance takes place after denrite parameters. Highest tensile strengths are obtained with large denrites and higher interaction areas, lowest tensile strengths are obtained when the denrites are short and weak in interaction. Despite the high eutectic cell count observed in eutectic and hypereutectic alloys, because these alloys solidify without precipitation of austenite denrites, their tensile strength values were found to be approximately half of the hypoeutectic alloys, which is one of the most important results regarding the importance laid on denrites in relationship with strength of cast irons.

2. Tensile strength values are found be clearly influenced from the composition of cast iron. Higher carbon equivalent values result in more carbon precipitated during solidification and hence, lower strength values. Conversely, lower carbon equivalents result in more primary austenite, reduced carbon precipitation during eutectic solidification and higher tensile strength values.

3. The graphite type formed in a cast iron is not a direct result of the effect of carbon equivalent or minimum eutectic temperature but combination of many internal parameters such as primary solidification, eutectic solidification, undercooling, and external parameters such as composition and inoculation, that affect the whole solidification process.

4. There found to be clear relationships between the composition of the alloy and temperature of austenite liquidus. It can be concluded that temperature of austenite liquidus can be used as pratical evaluation tool for predicting the composition of gray cast iron. A more consistent result for CEL value than the formula of Multi-Lab Quik-Cup is suggested, which is;

   CEL = 17,15 – 0,0111(TAL)

5. Statistical dependence of the total effect of composition and inoculation on temperature of eutectic nucleation and eutectic recalescence were also found to be significant.

6. No significant relationships could be established between the heat of primary solidification and secondary dendrite arm spacing, and heat of eutectic solidification end eutectic cell count. This result arises from the fact that heats of primary and eutectic solidification indicates the bulk amount of austenite and eutectic formed and do not provide any indication on the number of dendrites or eutectic cells. Also no significant relationships between the eutectic cell density and the minimum eutectic temperature could be established.

7. Examination of relevance of A1 and A2 areas on eutectic cell count yielded a very weak relation for A1 area, whereas A2 area has found to have no relation at all.

REFERENCES

1. M. J. Oliviera, L. F. Malheiros, C.A. Silva Ribeiro, "Evaluation of Heat of Solidification of Cast Irons From Continious Cooling Curves", Journal of Materials Processing Technology, 1999

2. R. A. Hardling, N. J. Saunders, "Theory and Practice of Computer Modelling of Phase Diagrams for Cast Irons", AFS Transaction, 451

3. Ernest J. Teichert, Ferrous Metallurgy, Volume III, 1944, 131, 530

4. William Hume - Rothery, G. V. Raynor, The Structure of Metals and Alloys, 1962, 286, 290

5. Howard E. Boyer, Timothy L. Gall, Metals Handbook Desk Edition, Volume 1, 1985, 5.3

6. I. Minkoff, Solidification and Cast Structure, 1986, 192, 194, 198, 199, 207, 208

7. B. Lux, W. Kurz, "Eutectic Growth of Iron – Carbon – Silicon and Iron – Carbon – Silicon – Sulphur Alloys", The Solidification of Metals, 1968, 193

8. Elkem, Cast Iron Inoculation, The Technology of Graphite Shape Control, 1997, 2

9. H. L. Morgan, Inoculation of Cast Iron, BCIRA, 1984, 339
10. W. Kurz, D.J. Fisher, Fundamentals of Solidification, 1992, 28

11. Rudolf Sillén, Ralf Lisell, "Optimization of Inoculation Practice by Means of Thermal Analysis", Novacast, 1999

12. Elkem, Cast Iron Inoculation, The Technology of Graphite Shape Control, 1997, 2

13. J. R. Brevick, J. Davis, "Applying Delta T Measurements to Gray Iron Inoculation", AFS Transactions, 379

14. I. Minkoff, The Physical Metallurgy of Cast Iron, 1983, 81

15. M. Hillert and Subba Rao V. V., "Gray and White Solidification of Cast Iron", The Solidification of Metals, 1968, 204

16. R. W. Heine, "The Fe – C Transformation Diagram Related to Solidification of Cast Irons", AFS Transactions, 187

17. D. Glover, C. E. Bates, R. Monroe, "The Relationships Among Carbon Equivalent, Microstructure and Solidification Characteristics and Their Effects on Strength and Chill in Gray Cast Iron", AFS Transactions, 745

18. Long-Sun Chao, Wu-Chang Du, "Macro-Micro Modelling of Solidification", National Science Council, ROC (A), Vol. 23, 1999, 622

19. T. Mizoguchi, J. H. Perepezko, C. R. Loper, Jr., "Nucleation During Solidification of Cast Irons", AFS Transactions, 89

20. D. M. Stefanescu, F. Martinez, I. G. Chen, "Solidification Behaviour of Hypoeutectic and Eutectic Compacted Graphite Cast Irons. Chilling Tendency and Eutectic Cells", AFS Transactions, 205

21. Frans Mampaey, "A Comparative Study of Nucleation in Lamellar and Spheroidal Graphite Cast Iron", Modelling of Casting, Welding and Advanced Solidification Processes V, The Minerals, Metals and Materials Society, 1991, 403

22. David D. Goettsch, Jonathan A. Dantzig, "Modelling Microstructure Development in Gray Iron Castings", Modelling of Casting, Welding and Advanced Solidification Processes V, The Minerals, Metals and Materials Society, 1991, 377

23. Joel Hemanth, "Effect of Sub-Zero (Cryogenic) and Water-Cool Chilling on Solidification and Mechanical Behaviour of Cast Iron", Materials Science and Engineering, 2001, 244

24. Suli Chang, Dongkai Shangguan, D. M. Stefanescu, "Modelling of the Liquid/Solid and the Eutectoid Phase Transformations in Spheroidal Graphite Cast Iron", Metallurgical Transactions A, 1992, 1333

25. D. A. Porter and K. E. Easterling, Phase Transformations in Metals and Alloys, 1992, 214

26. Richard A. Flinn, Fundamentals of Metal Casting, 1963, 16

27. W. Van Der Perre, Eutectic Undercooling Measurement As a Means For Quality Analysis of Lamellar ann S. G. Iron, 1990, 2

28. L. E. Menawati, R. W. Heine, C. R. Loper Jr., "Relationship of Gray Iron Macro and Microstructure to Cooling Curves", AFS Transactions, 363

29. I. Minkoff, "How Do Cast Irons Solidify? A Rewiev of Micromodelling Using The Computer, Supporting Experiments and Basic Theory", The Foundryman, 1993, 16

30. I. C. H. Hughes, "A Review of Solidification of Cast Irons With Flake Graphite Structures", The Solidification of Metals, 1968, 184

31. M. Rappaz, Modelling of Microstructure Formation in Solidification Processes", International Materials Reviews, 1989, 93

32. I. G. Chen, D. M. Stefanescu, "Computer Aided Differential Thermal Analysis of Spheroidal and Compacted Graphite Cast Irons", AFS Transactions, 947

33. U. Ekpoom, R. W. Heine, "Thermal Analysis by Differential Heat Analysis (DHA) of Cast Iron", AFS Transactions, 1981, 27

34. H. L. Tsai, "Determination of Latent Heat Release and Its Effect on Casting Solidification", Modelling of Casting, Welding and Advanced Solidification Processes V, The Minerals, Metals and Materials Society, 1991, 545

35. F. J. Bradley, Cai Jun, M. H. Zmerli, "Numerical Simulation of the Solidification of Eutectic Ductile Iron Casting Alloys", Numerical Methods in Thermal Problems, Volume VI, 1989, 320

36. H. T. Angus, "Cast Iron: Physical and Engineering Properties", 1976

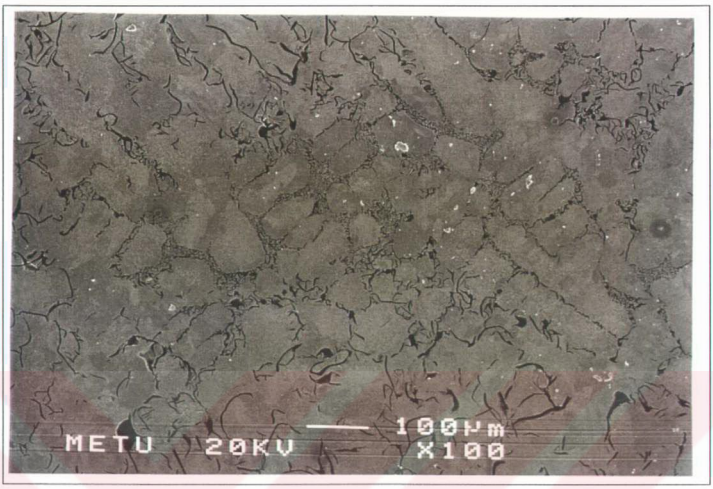

Figure 26. Type D in the middle surrounded by Type E in heat no. 172

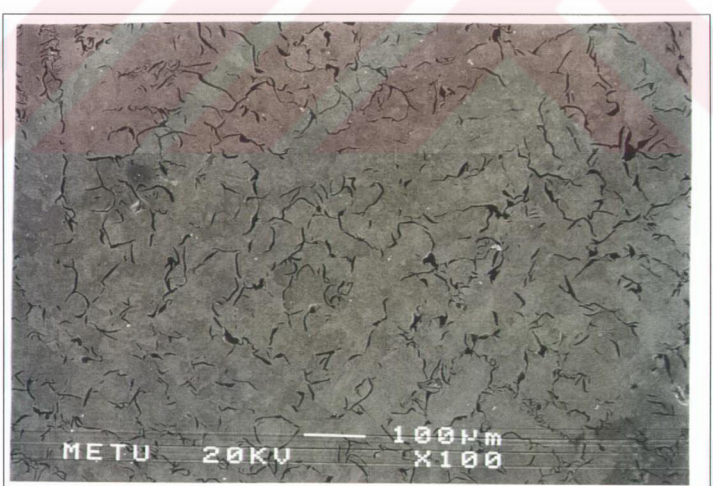

Figure 27. Type E flakes in heat no. 172

Figure 24. Type A flakes in heat no. 22

Figure 25. Type A (at left) and coarse Type C flakes in heat no. 62